

N71-14744  
NASA CR-115883

ROCKET BORNE ULTRAVIOLET SPECTROMETER MEASUREMENT  
OF  
OH RESONANCE FLUORESCENCE  
WITH  
A DIFFUSIVE TRANSPORT MODEL  
FOR  
MESOSPHERIC PHOTOCHEMISTRY

by

James G. Anderson

Laboratory for Atmospheric and Space Physics  
University of Colorado  
Boulder, Colorado 80302

CASE FILE  
COPY

\* Based on part of a thesis submitted to the University of Colorado for a Ph.D. in the Department of Astro-Geophysics.

Nicolet      Donahue      Leovy  
Hansen      Ferguson      Brinkmann

## ABSTRACT

An upper limit on the column density of the hydroxyl radical in the earth's upper atmosphere was determined with a rocket-borne scanning spectrometer using resonance fluorescence techniques in the near ultraviolet. The (0-0) band of the  $A^2\Sigma - X^2\Pi$  transition at 3064 Å was studied between 60 and 108 km under evening twilight conditions from Wallops Island, Virginia, 27 June 1969. The solar zenith angle was 92 degrees.

Particular attention is given to the problem of determining the Rayleigh scattered background to allow an accurate determination of the column emission rate from the OH molecule. An emission rate factor calculation for OH is presented which considers the rotational structure of the molecule and the effect of absorption by OH in the solar atmosphere. Using this emission rate factor the upper limit on the column density of OH is found to be  $6 \times 10^{12} \text{ cm}^{-2}$  at 65 km,  $3 \times 10^{12} \text{ cm}^{-2}$  at 75 km and  $7 \times 10^{11} \text{ cm}^{-2}$  at 85 km.

The dissociation rate for water vapor was calculated using a high resolution analysis of the O<sub>2</sub> absorption cross section. A significant amount of H<sub>2</sub>O dissociation was found to occur throughout the mesosphere down to the stratopause. A mesospheric oxygen-hydrogen model which includes diffusive transport of water vapor and the recalculated H<sub>2</sub>O dissociation rate is considered in order to interpret the experimental results.

It is demonstrated that the upper limit on the hydroxyl column density requires the eddy diffusion coefficient to be less than  $4 \times 10^6 \text{ cm}^2/\text{sec}$  in the lower mesosphere. A model for the concentration of H, OH, HO<sub>2</sub> and H<sub>2</sub>O in the mesosphere is presented using a water vapor mixing ratio of  $5 \times 10^{-6}$  at 50 km and an eddy diffusion coefficient of  $1 \times 10^6 \text{ cm}^2/\text{sec}$ .

## INTRODUCTION

Discovery of the hydroxyl vibration-rotation bands by Meinel (1950) provided the first direct observational evidence for the existence of reactive hydrogen species in the mesosphere of the earth. Rocket-borne measurements of OH infrared emission (see for example Packer, 1961 or Tarasova, 1963) have since located the peak intensity at about  $80 \pm 3$  km. While these infrared emission features demonstrate the existence of OH in the upper atmosphere, it is presently impossible to determine a density profile from the volume emission rate because of several problems:

- (1) The emitted intensity is more indicative of the rate of formation of OH than of its actual density, as the primary mechanism is  $H + O_3 \rightarrow OH^* + O_2$ .
- (2) The relative effectiveness of the formation mechanisms for populating the various vibrational levels is unknown.
- (3) Little agreement exists regarding the number of photons emitted from each excited molecule as it cascades to the ground level.
- (4) The radiative lifetimes of the vibrational transitions are not accurately known.

Resonance fluorescence by OH after absorption of solar radiation in the ultraviolet removes these ambiguities, because the energy required ( $\sim 4$  ev) precludes thermal or chemical excitation. For the purpose of studying the fluorescent emission, an ultraviolet scanning spectrometer was launched aboard a sounding rocket to determine the OH column emission rate resulting from the (0-0) vibrational band of the  $A^2\Sigma - X^2\Pi$  electronic transition at 3064 Å. A spectral resolution of 4 Å and a full wavelength scan once each kilometer

from the commencement of data acquisition at 58 km to apogee at 108 km significantly improved both the spectral and altitude resolution of the experiment over that of previous airglow surveys. The optical axis of the instrument was aligned approximately in the zenith direction; the launch took place under evening twilight conditions.

To relate the column emission rate to a column density using this method, it is necessary to calculate the "emission rate factor" for resonance fluorescence, which is a product of the excitation source intensity (in this case the solar flux) and the appropriate scattering cross section. Calculation of the emission rate factor thus requires knowledge of the oscillator strength of the vibrational transition, the rotational line strengths and the solar flux at each rotational line. A data reduction technique was developed to determine the Rayleigh scattered background independent of the spectrometer data which in turn allowed an upper limit on the OH column density to be determined as a function of altitude.

To interpret the experimental results, the species OH, H, HO<sub>2</sub> and H<sub>2</sub>O were first classified into two groups according to their characteristic lifetime against destruction. Water vapor is shown to have a lifetime significantly longer than the characteristic diffusion time indicating that its density profile is dictated by transport processes. However, OH, H and HO<sub>2</sub> have characteristic lifetimes less than the diffusion time in the region between 65 and 85 kilometers and are treated by photochemical equilibrium techniques.

Diffusive transport of H<sub>2</sub>O is regarded as the primary source of mesospheric water vapor and chemical production from reactions involving HO<sub>2</sub>, H and OH is shown to be insignificant. Models for H<sub>2</sub>O densities between 50 and 100 km are presented for eddy diffusion coefficients between  $2 \times 10^5$  and  $4 \times 10^6 \text{ cm}^2/\text{sec}$  and

mixing ratios of  $3 \times 10^{-6}$ ,  $5 \times 10^{-6}$  and  $7 \times 10^{-6}$  at 50 km. Because the chemical production of  $\text{H}_2\text{O}$  is assumed to be small, the diffusive transport solution becomes mathematically separable and can be solved without regard for the H, OH and  $\text{HO}_2$  densities. The major loss of  $\text{H}_2\text{O}$  is shown to result from photodissociation ( $\text{H}_2\text{O} + h\nu \rightarrow \text{OH} + \text{H}$ ) and reaction with  $\text{O}(^1\text{D})$ , ( $\text{H}_2\text{O} + \text{O}(^1\text{D}) \rightarrow \text{OH} + \text{OH}$ ) which constitutes the ultimate source of reactive hydrogen constituents in the earth's upper atmosphere. For this reason, it is necessary to establish a physically meaningful water vapor model before considering the hydrogen photochemistry. A fundamental improvement in the analysis is a recalculation of the water vapor photodissociation rate using the effective absorption cross section data for the Schumann-Runge band system determined as a function of column density by Hudson et al., (1969). These calculations demonstrate that a significant amount of solar radiation penetrates to the stratopause in the wavelength region between 1800 and 2000 Å.

The theoretical OH profiles which result from the analysis are integrated to correlate them as a function of altitude to the experimental results. It is demonstrated that the OH upper limit establishes an upper limit on the eddy diffusion coefficient and that the water vapor required for noctilucent clouds and water vapor ions at 80 km, coupled with the total available  $\text{H}_2\text{O}$  at 35 km suggests a quantitative lower limit on the diffusion coefficient. A resulting model is then presented which includes the  $\text{H}_2\text{O}$ , OH, H and  $\text{HO}_2$  number densities between 65 and 85 kilometers.

## II THE EXPERIMENT

A Nike-Apache rocket was launched from Wallops Island, Virginia, on June 28, 1969, at 00:36 GMT, to measure the hydroxyl ultraviolet airglow under evening twilight conditions. From previous airglow studies it was apparent that the hydroxyl emission would not significantly exceed the intensity of Rayleigh scattered solar flux in the region between 55 and 85 km. Observations of the ultraviolet hydroxyl emission presented the particular problem of separating a band emission feature from atmospheric Rayleigh scattering in a spectral region of highly variable solar flux. The experiment therefore sought to improve significantly both the altitude resolution and the spectral resolution of the data over that of previous attempts. An analysis of the  $A^2\Sigma - X^2\Pi$  (0-0) transition at appropriate mesospheric temperatures indicated that a 4 Å spectral resolution was adequate to locate the peak of the emission feature required for a positive identification. The wavelength scan rate of the instrument was chosen to allow one complete scan each second giving an altitude resolution of 1 km or better throughout the flight.

In order to minimize the scattered light within the spectrometer, it is desirable to maximize the angle between the solar vector and the optical axis of the instrument. Also, in order to reduce the amount of light scattered back into the atmospheric layer in which the measurement is taken, the earth's surface should not be illuminated below the instrument. These requirements coupled with the desire to execute the experiment during daylight equilibrium conditions established the late afternoon launch window.

Because the atmosphere is not transparent in the near ultraviolet, it was necessary to consider the problem of tangential absorption along the slant path between the sun and the scattering molecules. The reduction in the solar flux due to  $O_3$ ,  $O_2$ ,  $N_2$  and

Rayleigh scattering were considered. By graphing the vertical optical depth versus altitude and employing the Chapman function, the slant optical depth was found as a function of altitude. Using the United States Standard Atmosphere (1966), the  $O_3$  densities of Krueger and McBride (1968), the  $O_3$  absorption cross sections of Inn and Tanaka (1953), the  $N_2$  cross sections of Tanaka (1955) and the Rayleigh scattering cross section from Goody (1964), simple geometry allowed the shadow height (that altitude above the earth's surface where the slant optical depth between the scattering molecule and the sun is unity) to be determined. The experiment commenced with a solar depression angle of  $1.44^\circ$  which corresponds to a shadow height of 48 km. The slant path absorption at 65 km and above, where the measurements were taken, was negligible.

The spectrometer employed the basic Ebert-Fastie optical system (Fastie 1952), with a focal length of 250 mm and a 4096 square mm grating. The instrument may conventionally be viewed in three parts: (1) a detector head that houses the photomultiplier tube, the electrometer and the high voltage supply for the photo-tube; (2) the spectrometer chamber with associated optics and; (3) a bulkhead section that houses the 28 volt internal power source and all electronics exclusive of the electrometer. A bialkali cathode photomultiplier with a quantum efficiency of approximately 20% at  $3100 \text{ \AA}$  was used (ASCOP Model 542N-01).

The photomultiplier tube was calibrated using a tungsten filament at a known temperature, with a pass band filter to isolate

the wavelength. Comparison between the pyrometer used in the temperature determination and a NBS temperature standard indicates a pyrometer accuracy of  $\pm 10^{\circ}\text{K}$ . The transmission of the filter, calibrated at the National Center for Atmospheric Research is known to a precision of  $\pm 3\%$ . Uncertainties in the dimensions of the optical system used in the absolute calibration coupled with nonlinearities in the voltage measurement devices establishes an accuracy of  $\pm 20\%$  for the detector head calibration at  $2972 \text{ \AA}$ . The relative response of the tube (determined using sodium salicylate) and uncertainties in the determination of the optics transmission result in an instrument calibration accuracy of  $\pm 28\%$  at  $3100 \text{ \AA}$ . This error limit will be referred to in the presentation of the data in the next section.

## DATA REDUCTION

It was apparent at the conception of this experiment that a very accurate removal of the Rayleigh scattered background signal was necessary in order to realize an accurate determination of the OH column emission rate. There were two problems of particular concern. The first results from the highly variable solar flux in the instrument's scan region at the spectral resolution necessary to make a positive wavelength identification of the  $A^2\Sigma \rightarrow X^2\Pi$  (0-0) band of the hydroxyl radical. The second problem is created by the inherent polarization of the Rayleigh scattered radiation. Because the instrument's grating transmits with an efficiency that depends upon the angle between the electric vector of the radiation and a given vector in the focal plane of the instrument, the data are modulated with a period corresponding to the roll rate of the rocket.

The response of the instrument to the polarized radiation is treated by considering a coordinate system defined by a unit vector along the optical axis of the instrument and a unit vector originating at the scattering molecule pointing in the direction of the sun. The theory of small particle scattering (Goody, 1964), is then used to relate the electric vectors perpendicular to and parallel to the scattering plane before and after the wave interacts with the atmospheric particle. The scattered wave is considered as two perpendicular electric vectors and the instrumental response function is determined by considering the transmission of these vectors separately through the instrument.

The optics transmission is carried out using unpolarized light and therefore the photometric equation

$$S = \frac{[4\pi f]}{4\pi} \frac{A_s A_g \cos\theta_e}{f^2} T_{U.P.} \quad (1)$$

must be corrected, where:

- S is the signal strength in photons/sec leaving the instrument's exit slit,  
[ $4\pi I$ ] is the observed source intensity,  
f is the instrument's focal length,  
 $A_g$  is the area of the grating,  
 $A_s$  is the slit area,  
 $\theta_e$  is the angle between the incident light and the grating normal.  
 $T_{U.P.}$  is the unpolarized transmission function.

The correction is accomplished by multiplying the right hand side of equation (1) by a function  $F(\theta, \alpha, \lambda) = T(\theta, \alpha, \lambda)/T_{U.P.}(\lambda)$  that corrects for the instruments sensitivity to orientation with respect to the scattering plane ( $\alpha$ ) and to the angle between the optical axis and the solar vector ( $\theta$ )

The parameter which specifies the degree of instrumental polarization is commonly designated P and is defined by

$$P = \frac{I_M - I_m}{I_M + I_m}$$

where  $I_M$  and  $I_m$  are the maximum and minimum measured intensities of linearly polarized light with electric vectors oriented along the maximum and minimum axis of the instrument's acceptance ellipse.

The correction function  $F(\alpha, \theta, \lambda) = F(\gamma, \delta, \theta, \lambda) = T(\gamma, \delta, \theta, \lambda)/T_{U.P.}(\lambda)$  where  $\alpha = \delta + \gamma$  is given (Anderson and Meira, 1969) by

$$F(\gamma, \delta, \theta, \lambda) = 1 - P \left[ \frac{(1-\Delta) + (\Delta-1) \cos^2 \theta}{(\Delta+1) + (1-\Delta) \cos^2 \theta} \right] (\cos 2\gamma \cos 2\delta + \sin 2\gamma \sin 2\delta) \quad (2)$$

The angle  $\delta$  is measured from a unit vector parallel to the instrument's entrance slit in the focal plane of the instrument to a unit vector parallel to the major axis of the instrument's acceptance ellipse.  $\gamma$  is the angle between a unit vector parallel to the instrument's entrance slit in the focal plane of the instrument and a unit vector perpendicular to the scattering plane defined by the instrument's optical axis and the unit vector pointing in the solar direction from the scattering center. By symmetry arguments  $\delta$  must be either  $90^\circ$  or  $0^\circ$  because the grating rulings which polarize the light are parallel to the entrance slit of the spectrometer.  $F(\gamma, \delta, \theta, \lambda)$  is generally dependent implicitly on time through the angle  $\gamma$  as the rocket rotates about its roll axis at several revolutions per second. The roll channel of the gyro supplies  $\gamma(t)$  throughout the flight so the exact orientation of the entrance slit of the spectrometer with respect to the scattering plane is known at all times.  $P$  and  $\delta$  are determined in the laboratory prior to flight by using a tungsten lamp and a polarization plate that linearly polarizes the lamp's radiation. The instrument is rotated with respect to this laboratory system to determine  $P$  and  $\delta$ .

The number of photons striking the cathode of the photomultiplier may then be written

$$S = \frac{[4\pi\vartheta]}{4\pi} \frac{A_s A_e \cos \theta_e}{f^2} T_{U.P.}(\lambda) \left\{ 1 - P \left[ \frac{(1-\Delta + (\Delta-1)\cos^2 \theta)}{(\Delta+1 + (1-\Delta)\cos^2 \theta)} \right] \cdot (\cos 2\gamma \cos 2\delta + \sin 2\gamma \sin 2\delta) \right\}$$
(3)

The column emission rate [ $4\pi J$ ] of the Rayleigh scatter is:

$$4\pi J_{RAY} = \pi F_0 \sigma_{RAY} (\eta/\mu) P(\cos \theta) \quad (4)$$

where

$\pi F_0$  is the incident solar flux,

$\eta$  is the atmospheric column density,

$\mu$  is the slant column correction  $\cos \chi$ ,

$\sigma_{RAY}$  is the Rayleigh scatter cross section,

$P(\cos \theta)$  is the scattering phase function for

Rayleigh scattering.

For unpolarized incident radiation the phase function is (Goody, 1964)

$$P(\cos \theta) = \frac{3}{2(2+\Delta)} \left\{ 1 + \Delta + (1-\Delta) \cos^2 \theta \right\}$$

The depolarization factor,  $\Delta$ , is determined empirically and is equal to .035 for dry air (Goody, 1964).

The Rayleigh background signal is then obtained by substituting

(4) into (3) to give

$$S = \frac{(4\pi\eta_0)\sigma_{RAY}}{4\pi} (\eta/\mu) \left\{ \frac{3}{2(2+\Delta)} [1+\Delta+(1-\Delta)\cos^2\theta] \right\}$$

$$\frac{A_s A_g \cos \theta_e}{f^2} T_{U.P.}^{(\lambda)} \left\{ 1 - P \left[ \frac{(1-\Delta)+(\Delta-1)\cos^2\theta}{(\Delta+1)+(1+\Delta)\cos^2\theta} \right] \right\} \quad (5)$$

$$[\cos 2\gamma \cos 2\delta + \sin 2\gamma \sin 2\delta] \}$$

When applying this equation to a particular experiment, the initial step is to replace the independent variable  $z$  in the column density of the main atmosphere  $\eta(z)$  with  $t$ , the time measured from launch. This was done by using a 5th degree polynomial fit of the rocket's trajectory correlated with a standard atmosphere (CIRA, 1965). The solar flux is determined by passing the triangular slit function of the instrument over the high (.05 Å) resolution data (Brückner, 1960) digitized by Furukawa et al. (1967).

It should be recognized that all quantities on the right hand side of equation 5 are independent of the spectral data taken during the rocket experiment.  $S$  is calculated each millisecond throughout the flight and a magnetic tape is then generated with each spectral scan of the instrument reproduced with the Rayleigh scattered background in place of the actual flight data. Figure 1 shows an example of the background construction compared to the actual spectrometer data at an altitude of 69 km. A data frame from the flight similar to Figure 1 exists for each kilometer of the atmosphere between 60 and 90 kilometers, above which the signal

becomes less than the photomultiplier noise level. At this point in the data reduction the following points were apparent:

- (1) The major details of the Rayleigh scattered background present in the flight data are reproduced in the constructed data.
- (2) Examination of the thirty data frames between 60 and 90 kilometers revealed that the experimental data had the same apparent scale height as the atmosphere.
- (3) Absolute intensity agreement was achieved by multiplying the constructed background by 1.15; the constant was independent of altitude and of wavelength.
- (4) The amplitude and phase of the roll induced modulation in the spectrometer data is faithfully reproduced in the constructed background.
- (5) The solar flux data used in the background construction (taken with a spectrograph) has some apparent film blemishes that appear as emission features not present in the photoelectric data taken during the flight.

Each wavelength scan above 65 km was analyzed by subtracting the constructed background from the flight data. The wavelength interval in the vicinity of 3090 Å was then examined to establish the maximum difference between the constructed background and the spectrometer data at the peak intensity of the OH transition. This resulted in the experimental determination of an upper limit on the column emission rate of the hydroxyl radical shown in Figure 2.

The emission rate factor, which is the proportionality factor between the column emission rate and the column density, was calculated by considering the rotational transitions of the molecule from  $K = 1$  to  $K = 30$ , where  $K$  is the total angular momentum apart from spin for each of the 12 branches in the vibrational band. The calculation assumed that

the molecule was in the ground vibrational level of the  $X^2\Pi$  (ground) state. This approximation is accurate to about one percent if the quite reasonable assumption is made that each OH molecule is created in an excited vibrational state and that an average of 4 transitions occur with a radiative lifetime of  $10^{-2}$  seconds, as the lifetime of OH is approximately 5 seconds in the lower and middle mesosphere. The emission rate factor for the entire band was calculated to be  $4.3 \times 10^{-3}$  photons/sec.

Errors inherent in the calculations are important. As mentioned in the introduction, the oscillator strength for the band and the solar flux at each rotational line in the band must be known. The oscillator strength of Golden et al. (1963) of  $7.1 \pm 1.1 \times 10^{-4}$  contributes an error of  $\pm 16\%$  and the solar flux values contribute  $\pm 20\%$  (Furukawa et al. 1967). However, an additional problem is created by the existence of OH at the temperature minimum in the solar atmosphere which must be accounted for by an accurate reconstruction of the Fraunhofer structure. The ground based data of Brückner (1960) taken with an instrument of half width equal to 33  $m\text{\AA}$  were corrected for instrumental broadening and the depths of the absorption lines were determined to within  $\pm 5$  percent. Therefore, when the emission rate factor with its associated error bar is divided into the column emission rate the resulting column density is accurate to  $\pm 65$  percent. The resulting upper limit is displayed as a function of altitude in Figure 3 with the experimental error shown by the error bars to the right of the measurement. The remainder of the discussion will focus on the interpretation of this upper limit.

## THE ROLE OF UPPER ATMOSPHERIC WATER VAPOR

A distinguishing characteristic of oxygen-hydrogen chemistry in the mesosphere is that all of the hydrogen species may be classified into two distinct groups according to their lifetime against destruction. Water vapor and molecular hydrogen are stable and possess lifetimes exceeding the characteristic diffusion time  $H^2/D_E$ , where  $H$  is the constituent scale height and  $D_E$  is the eddy diffusion coefficient. This implies that one must account for the transport of  $H_2O$  and  $H_2$  between different altitude regions if a physically meaningful result is to be expected. On the other hand  $H$ ,  $OH$  and  $HO_2$  are easily oxidized by either atomic oxygen or ozone which establishes a strict internal photochemical equilibrium between the three constituents. The reaction between  $H$  and  $HO_2$  which forms  $H_2$  is sufficiently rapid to insure that the  $H - OH - HO_2$  system remains in photochemical equilibrium throughout the mesosphere, (a poor assumption above 80 km). Under equilibrium conditions the  $OH$ ,  $H$  and  $HO_2$  densities may be determined by equating the chemical production and loss terms, neglecting transport effects altogether. This separation according to characteristic lifetime is a central feature of the chemistry presented in the sections that follow.

An analysis of the chemical reactions recycling  $H_2O$  from  $H$ ,  $HO_2$  and  $OH$  show them to be incapable of maintaining significant amounts of water vapor at altitudes much above 65 km. A key result of this is that if water is present at the mesopause it must be transported there, probably by eddy diffusion. As higher altitudes in the mesosphere are considered the increasingly insignificant  $H_2O$  production from  $H$ ,  $HO_2$  and  $OH$  also means that the problem may be separated mathematically because the continuity equation for water vapor may be solved without

regard for the H, OH and HO<sub>2</sub> densities. Therefore, the problem of mesospheric hydrogen chemistry will be approached by first establishing a realistic model for water vapor.

Molecular hydrogen is also controlled by diffusion, but it is so stable (lifetime  $\sim 10^7$  sec) that its formation by the reaction H + HO<sub>2</sub> = H<sub>2</sub> + O<sub>2</sub> effectively removes the hydroxyl and perhydroxyl molecule permanently from the hydrogen reaction scheme. H<sub>2</sub> may thus be disregarded as an active partner in the production of H<sub>2</sub>O, H, OH and HO<sub>2</sub>.

The total amount of water vapor available at the stratopause has been the subject of a number of studies, both experimental (see for example Mastenbrook, 1968) and theoretical (for example Nicolet, 1964). Although the exact mixing ratio at 50 km is not known, it is felt that a range of values between 3 and 7 parts per million adequately encompasses the range of probable values. An analysis of the dependence of the calculations to be presented upon the particular mixing ratio chosen will show that the diffusion coefficient is the critical parameter determining upper mesospheric water content and not the particular mixing ratio chosen at the 50 km level. In order to establish a water vapor model, the loss processes will be examined first.

TABLE I

Wavelength Interval	Resolution	Source
1214 - 1217 Å	.015 Å	Bruner and Rense (1969)
900-1550 Å	.2 Å	Brinkmann et al. (1966)
1550-1760 Å	50 Å	Hinteregger et al. (1965)
1760-2060 Å	.2 Å	Brinkmann et al. (1966)
2060-2100 Å	.1 Å	Furukawa et al. (1967)

## H<sub>2</sub>O LOSS PROCESSES

Two dissociation mechanisms, photodissociation and reaction with O(<sup>1</sup>D), are thought to predominate in the destruction of water vapor above the stratosphere. A calculation of the H<sub>2</sub>O photodissociation rate using recently determined effective O<sub>2</sub> Schumann-Runge band absorption cross sections measured as a function of column density demonstrates that photodissociation is significant throughout the mesosphere, dominated by O(<sup>1</sup>D) below perhaps 60 km.

Incident solar photons dissociate water vapor at a rate given by

$$J_{H_2O}(z) = \sum \frac{[\pi \mathcal{I}_0(\lambda)]}{\pi} \sigma_{H_2O}(\lambda)$$

$$\cdot \exp [ - (\eta_{O_3}(z) \sigma_{O_2} + \eta_{O_3}(z) \sigma_{O_3} + \eta_{H_2O}(z) \sigma_{H_2O}) ]$$

where

[ $\pi \mathcal{I}_0(\lambda)$ ] is the solar flux at the top of the atmosphere reduced by a factor of  $\pi$  to average over the earth's rotation (lifetime of water vapor significantly exceeds one day)

$\sigma$  is the absorption cross section

$\eta(z)$  is the column density above height z

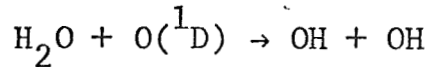
The calculation was carried out in 10 Å intervals from 900 to 2100 Å between 50 and 100 km in 1 km intervals. The solar flux data were taken from the sources listed in Table I. With the exception of the region near the Schumann-Runge band system, a running average was

taken over each  $10 \text{ \AA}$  interval and that value was assigned to the central wavelength in the region. Table II represents a tabulation of the absorption cross section sources used in the calculation. The particularly critical region in the cross section determination is for wavelengths greater than  $1750 \text{ \AA}$  for  $\text{O}_2$  absorption in the Schumann-Runge band system. This can be understood by examining the wavelength dependence of the absorption cross sections for  $\text{O}_2$  and  $\text{H}_2\text{O}$  in Figure 4. The penetration of effective solar energy into the mesosphere is constrained to the very narrow interval between  $1800 \text{ \AA}$  and about  $2050 \text{ \AA}$ , above which the  $\text{H}_2\text{O}$  cross section become negligibly small. This wavelength region has been studied in detail (see for example Thompson et al., 1963; Watanabe, 1958; Blake et al., 1966). However, an investigation of the column density dependent effective cross section for  $\text{O}_2$  in the Schumann-Runge band system was carried out by Hudson et al., (1969) in a study of atomic oxygen production from  $\text{O}_2$  in the atmosphere of the earth. The effective cross section was found to be a distinct function of column density at  $\text{O}_2$  optical depths encountered between 50 and 100 kilometers in the earth's upper atmosphere. The original attenuation data kindly supplied by Hudson (1970), were used to calculate the effective cross sections presented as a function of altitude in Figures 5 to 8. The conversion from altitude to column density employed the U.S. Standard Atmosphere (1966)  $\text{O}_2$  model.

TABLE II

Wavelength Interval	Reference
1214-1217 Å	Watanabe (1958)
900-1750 Å	Watanabe (1958)
1750-1973 Å	Hudson et al. (1969)
1973-2200 Å	Ditchburn and Young (1962)

Accounting for this column density dependence results in significantly larger values for the water vapor dissociation rate,  $J_{H_2O}$ , in the lower mesosphere when compared with dissociation rates calculated using averaged cross sections for  $O_2$  determined at only one column density. To demonstrate this the spectral region between 900 Å and 2200 Å was broken into 5 subdivisions: 900 - 1214 Å, Lyman-alpha (1214 - 1217 Å), 1217 to 1750 Å, the Schumann-Runge band region between 1750 and 1973 Å and the continuum from 1973 to 2200 Å. The contribution to the water vapor dissociation rate for each region is plotted in Figure 9. Figure 10 displays the sum of all spectral regions and compares that sum to a low resolution survey similar to that used by Hesstvedt (1968). Also included in Figure 10 is a plot of the  $O(^1D)$  concentration times  $10^{-10} \text{ cm}^3/\text{sec}$  which is the rate coefficient (Nicolet, (1970)) appropriate to



The sum of the dissociation rate and the rate of  $H_2O$  destruction by  $O(^1D)$  may be termed the loss coefficient for water vapor  $J'$  where:

$$J'_{H_2O} = J_{H_2O} + (10^{-10} \text{ cm}^3/\text{sec}) [O(^1D)] .$$

This loss function is also displayed in Figure 10 and will be used to determine the water vapor concentration profile in the section that follows.

TABLE III

Reaction	Rate Coefficient	Source
$\text{OH} + \text{HO}_2 \rightarrow \text{H}_2\text{O} + \text{O}_2$	$k = 1 \times 10^{-11} \text{ cm}^2/\text{sec}$	Kaufman, (1964)
$\text{OH} + \text{H}_2\text{O}_2 \rightarrow \text{H}_2\text{O} + \text{HO}_2$	$4 \times 10^{-13} \text{ cm}^2/\text{sec}$	Foner and Hudson, (1962)
$\text{OH} + \text{OH} \rightarrow \text{H}_2\text{O} + \text{O}({}^3\text{P})$	$2 \times 10^{-12} \text{ cm}^2/\text{sec}$ (5-11)	Westenberg and de Hass, (1965)
$\text{H} + \text{OH} + \text{M} \rightarrow \text{H}_2\text{O} + \text{M}$	$2.5 \times 10^{-31} \text{ cm}^6/\text{sec}$	Kaufman, (1964)
$\text{H}_2 + \text{OH} \rightarrow \text{H}_2\text{O} + \text{H}$	$1 \times 10^{-10} \exp(-5.9/kT) \text{ cm}^3/\text{sec}$	Kaufman, (1964)

## A DIFFUSIVE SOLUTION FOR MESOSPHERIC WATER VAPOR

Three basic assumptions define the solution to be examined :

- (1) Diffusive transport upward from the stratopause constitutes the major source of mesospheric water vapor.
- (2) The losses through photolysis and reaction with  $O(^1D)$  represent the major sink for  $H_2O$  molecules.
- (3) The characteristic lifetime of water vapor is sufficiently long that its diurnal variation is negligible.

Chemical reactions that recycle the reactive hydrogen constituents into water vapor are listed in Table III. They are incapable of replenishing water vapor to any meaningful degree above 65 km. (This approximation was checked using the model for OH, H and  $HO_2$  presented in the next section. The chemical equilibrium density of  $H_2O$  amounted to .45 of that presented in the model at 65 km and .09 at 75 km.)

The diffusion equation for water vapor was numerically integrated on a digital computer using an improved second order Runge-Kutta method (see McCalla, 1967). Several cases were investigated, with constant eddy diffusion coefficients of  $4 \times 10^6$ ,  $1 \times 10^6$  and  $2 \times 10^5 \text{ cm}^2/\text{sec}$ . The solutions were obtained between 50 and 100 km in increments of .5 km. Boundary conditions were chosen such that the gradient of the mixing ratio always remained negative (sources only at the lower boundary), the mixing ratio always remained positive and the flux of molecules entering the lower boundary equaled the total number of molecules dissociated between the lower boundary and infinity. Mixing ratios at 50 km of 3, 5 and 7 parts per million are presented in Figures 11, 12 and 13 respectively. The destruction

coefficient  $J'$  in Figure 10 was used in all cases.

The solutions exhibit some notable characteristics. It is apparent first of all that the critical quantity determining the  $H_2O$  distribution in the upper mesosphere is the diffusion coefficient and not the particular value chosen for the mixing ratio at 50 km. In fact, for an eddy diffusion coefficient of  $2 \times 10^5 \text{ cm}^2/\text{sec}$ , the atmosphere at 80 km is nearly devoid of water for all three mixing ratios considered. Calculations showed that a coefficient of approximately  $6 \times 10^5 \text{ cm}^2/\text{sec}$  or greater is required if any water vapor is to be present at the mesopause. It is therefore unrealistic to assume an approximately constant  $H_2O$  mixing ratio up to 75 km without invoking a transport model.

Examination of Figures 11 - 13 also demonstrates that for an eddy diffusion coefficient of  $2 \times 10^5 \text{ cm}^2/\text{sec}$ , the mixing ratio gradient at 50 km is large for all three solutions. This presents an interesting inconsistency in that for a coefficient of  $2 \times 10^5$  a much larger water vapor concentration would result at the 40 km level (because of the rapid downward increase in the mixing ratio) than the total available  $H_2O$  supply will allow. Thus if a coefficient of  $2 \times 10^5$  is assumed, this dilemma can be resolved only by assuming that a significant reduction in the water vapor mixing ratio takes place between 35 km (the highest altitude of measured  $H_2O$  densities) and 50 km. Under these conditions, however, nearly total extinction of  $H_2O$  would occur by 70 km. On the other hand, the "strong" eddy diffusion case represented by a coefficient of  $4 \times 10^6 \text{ cm}^2/\text{sec}$  is seen to maintain a nearly constant mixing ratio between 50 and 100 km, as the ratio at 100 km is about

one-half that at 50 km.

The next section formulates the oxygen-hydrogen chemistry explicitly in terms of the water vapor density. The determination of an experimental upper limit on OH is used to constrain the eddy diffusion coefficient and the mixing ratio of H<sub>2</sub>O at the base of the mesosphere. Conclusions are drawn concerning HO<sub>2</sub> and H which are in equilibrium with OH throughout the 50 to 100 km region.

## INTERPRETATION OF EXPERIMENTAL RESULTS

Physically realistic treatments of the oxygen-hydrogen photochemistry all too often lead to numerical results that offer little physical insight into the hydrogen reaction system. Fortunately, as mentioned previously, alternative methods exist based upon separation of reacting species according to their lifetime against destruction. Figure 14 is a schematic of the major reactions involving  $H_2O$ , OH, H,  $HO_2$  and  $H_2$  and serves to demonstrate 3 important points:

- (1) The ultimate source of reactive hydrogen is the dissociation of  $H_2O$  shown by the arrows representing  $H_2O + h\nu \rightarrow OH + H$  and  $H_2O + O(^1D) \rightarrow OH + OH$  emanating from the lower lefthand corner of the diagram
- (2) Calculations show that the principal terminating reactions for OH, H and  $HO_2$  are  $HO_2 + H \rightarrow H_2 + O_2$  and  $HO_2 + OH \rightarrow H_2O + O_2$  which represent a net loss to the reactive hydrogen chain because in the first case molecular hydrogen is sufficiently stable to prevent recycling and in the second case the water vapor produced by OH and  $HO_2$  does not increase the available  $H_2O$  density to any significant extent. The reactions are rapid enough to keep the OH - H -  $HO_2$  system in chemical equilibrium with its environment.
- (3) Rapid oxidation reactions involving O and  $O_3$  along with the 3 body reaction  $H + O_2 + M \rightarrow HO_2 + M$  maintain a strict internal photochemical equilibrium between OH, H and  $HO_2$ . Each reaction forms another of the reactive hydrogen constituents creating a closed chain.

Table IV lists the reactions, reaction rates and reaction rate sources used in the chemical calculations for interpreting the data. Although the list is not complete, it does encompass all those reactions thought to be of any quantitative significance to the

TABLE IV

Rate Coefficient

Source

Reaction		Shimazaki (1969)
$O_2 + h\nu \rightarrow O(^3P) + O(^3P)$		Shimazaki (1969)
$O_2 + h\nu \rightarrow O(^1D) + O(^3P)$		Shimazaki (1969)
$O_3 + h\nu \rightarrow O(^1D) + O_2$		Shimazaki (1969)
$H_2O + h\nu \rightarrow OH + H$	$J_{H_2O}(1969) O_2$ cross section	calculated using Hudson et al.
$H_2O_2 + h\nu \rightarrow OH + OH$		Shimazaki (1969)
$O + O + M \rightarrow O_2 + M$	$k_1 = 3.0 \times 10^{-33}$	Campbell & Thrush (1967)
$O + O_2 + M \rightarrow O_3 + M$	$k_2 = 8.2 \times 10^{-35} \exp(-.89/RT)$	Kaufman & Kelso (1964)
$O + O_3 \rightarrow O_2 + O_2$	$k_3 = 5.6 \times 10^{-11} \exp(-5.7/RT)$	Schiff (1969)
$O(^1D) + O_3 \rightarrow O_2 + O_2$	$k_4 = 3 \times 10^{-11}$	Snelling & Bair (1967)
$O(^1D) + M \rightarrow O(^3P) + M$	$4.0 \times 10^{-11}$	Slanger et al. (1968)
$OH + O \rightarrow H + O_2$	$k_6 = 5 \times 10^{-11}$	Kaufman (1964)
$O_3 + H \rightarrow OH + O_2$	$k_7 = 2.6 \times 10^{-11}$	Kaufman (1964)
$H + M + O_2 \rightarrow HO_2 + M$	$k_8 = 3.0 \times 10^{-32}$	Schofield (1967)
$HO_2 + O \rightarrow OH + O_2$	$k_9 = 1 \times 10^{-11}$	Kaufman (1964)

TABLE IV (continued)

Reaction	Rate Coefficient	Source
$\text{HO}_2 + \text{H} \rightarrow \text{OH} + \text{OH}$	$k_{10} = 1 \times 10^{-11}$	Clyne and Thrush (1963)
$\text{HO}_2 + \text{O}_3 \rightarrow \text{OH} + 2\text{O}_2$	$k_{11} = 1 \times 10^{-14}$	Hunt (1966)
$\text{OH} + \text{O}_3 \rightarrow \text{HO}_2 + \text{O}_2$	$k_{12} = 5 \times 10^{-13}$	Kaufman (1964)
$\text{HO}_2 + \text{HO}_2 \rightarrow \text{H}_2\text{O}_2 + \text{O}_2$	$k_{13} = 1.5 \times 10^{-12}$	Kaufman (1964)
$\text{H}_2\text{O} + \text{O}(\text{I}_{\text{D}}) \rightarrow \text{OH} + \text{OH}$	$k_{14} = 1.0 \times 10^{-10}$	Nicolet (1970)
$\text{HO}_2 + \text{H} \rightarrow \text{H}_2 + \text{O}_2$	$k_{15} = 2.0 \times 10^{-13}$	Clyne & Thrush (1963)
$\text{HO}_2 + \text{OH} \rightarrow \text{H}_2\text{O} + \text{O}_2$	$k_{16} = 1 \times 10^{-11}$	Kaufman (1964)

$\text{OH}$ ,  $\text{H}$ ,  $\text{HO}_2$  and  $\text{H}_2\text{O}$  densities between 50 and 100 km. Although  $\text{H}_2\text{O}_2$  is included in the diagram and in the table for completeness, its quantitative effect upon  $\text{OH}$ ,  $\text{H}$  and  $\text{HO}_2$  was found to be negligible at all altitudes above 65 kilometers.  $\text{H}_2\text{O}_2$  is therefore not included in the photochemical solution.

The three equilibrium continuity equations for  $\text{OH}$ ,  $\text{H}$  and  $\text{HO}_2$  were solved in terms of water vapor as an independent variable. This is distinct from the alternative approach of analysing the dominant terms in the photochemical solution for  $\text{OH}$ ,  $\text{H}$  and  $\text{HO}_2$  which would result in a simplified system of equations not involving water vapor. Although the latter approach is mathematically correct as a approximation, it is not physically meaningful here because the cyclical reactions that establish the equilibrium between  $\text{H}$ ,  $\text{OH}$ , and  $\text{HO}_2$  create a dependence between the three species such that one must arbitrarily choose an altitude profile for one of the reactive hydrogen constituents in order to draw conclusions concerning the distribution of the remaining two. On the other hand, the distribution of  $\text{H}_2\text{O}$  is controlled by factors which are independent of the hydrogen chemistry as noted previously and a physically realistic solution for  $\text{H}_2\text{O}$  will result in  $\text{OH}$ ,  $\text{H}$  and  $\text{HO}_2$  profiles based upon their ultimate source.

The ozone distribution used in the calculation employed an empirically determined profile up to 55 km (Krueger and McBride, 1968), connected to a time dependent photochemical solution shown in Figure 15 resulting from the calculation of Park and London (1969). Also displayed in the same figure is the triplet P atomic oxygen profile resulting from the same time dependent calculation (Park and London, 1969). Both profiles correspond to equilibrium values appropriate to the flight time.

The nine water vapor altitude distributions calculated in the previous section corresponding to the three boundary conditions on the mixing ratio of  $H_2O$  at 50 km, with eddy diffusion coefficients of  $2 \times 10^5$ ,  $1 \times 10^6$  and  $4 \times 10^6 \text{ cm}^2/\text{sec}$  result in a manifold of 9 OH density profiles. These profiles were then integrated downward to determine the resulting OH column density as a function of altitude. Before comparing these calculations to the experimental results, two relationships should be noted:

- (1) An examination of figures 11 to 13 reveals that the water vapor concentration in the upper mesosphere is a direct function of the eddy diffusion coefficient.
- (2) The equilibrium photochemistry demonstrates that the density of OH is directly proportional to the square root of the water vapor concentration.

Therefore it follows that an upper limit on the effective eddy diffusion coefficient may be determined from an upper limit on the OH density, provided the OH upper limit is low enough to be physically meaningful.

Integrated OH profiles for the extreme diffusion coefficients considered in the study are shown in Figures 16, 17 and 18 for  $H_2O$  mixing ratios at 50 km of 3, 5, and 7 parts per million along with the experimentally determined upper limit on the OH column density. This demonstrates that the experimental upper limit is sufficiently low to exclude eddy diffusion coefficients equal to or larger than  $4 \times 10^6 \text{ cm}^2/\text{sec}$ . Noting that the abscissa in Figures 16 to 18 is logarithmic, it can be seen that as in the case of water vapor, the OH density in the middle and upper mesosphere is dependent more critically upon the eddy diffusion coefficient than upon the particular choice of a water vapor mixing ratio at the stratopause. In the discussion that follows, therefore, an upper limit of  $4 \times 10^6 \text{ cm}^2/\text{sec}$  for the eddy diffusion coefficient will be adopted.

The recalculated photodissociation rate for  $H_2O$  coupled with the transport solution for water vapor permits a semi-quantitative deter-

mination of the diffusion coefficient lower limit as follows. Examination of the water vapor mixing ratio profiles (Figures 11 to 13) reveals the large density gradient present at the 50 km level for  $D_{\text{eddy}} = 2 \times 10^5 \text{ cm}^2/\text{sec}$ , which implies significantly larger  $\text{H}_2\text{O}$  densities in the stratosphere because of the rapid downward increase in the mixing ratio. However, this violates the constraint established by the total amount of water available, determined within limits at 35 km by in situ measurements (Masterbrook, 1968). An alternative is to assume that the mixing ratio at the 40 to 50 km level does not represent the total amount of water vapor available (that is, a significant amount of water vapor has been removed between 35 and 50 km by dissociation) and that the mixing ratio is much less than one part per million at the stratopause. However, this conclusion would result in a mesosphere completely devoid of water vapor which contradicts the existence of such phenomena as water ion clusters (Narcisi, 1965, 1969; Ferguson, 1970), and noctilucent clouds (Chapman and Kendall, 1965; Witt, 1969). The eddy diffusion coefficient must be equal to or larger than  $5 \times 10^5 \text{ cm}^2/\text{sec}$  in the lower mesosphere to sustain those observed phenomena. Therefore, while no direct measurement of  $\text{H}_2\text{O}$  exists at the turbopause, the indirect evidence indicates that the diffusion coefficient must be greater than about  $5 \times 10^5 \text{ cm}^2/\text{sec}$  in the lower mesosphere.

It is not the intention of this study to present a complete model of the mesosphere, but the incorporation of the quantitative results into a model will serve to unify the calculations. An eddy diffusion coefficient of  $1 \times 10^6 \text{ cm}^2/\text{sec}$  is adopted using an  $\text{H}_2\text{O}$  mixing ratio of 5 parts per million at 50 kilometers. The distinguishing features of the model shown in Figure 19 are:

- (1) A column density dependent effective absorption cross section for  $\text{O}_2$  is included which allows the attenuation of incident solar energy to be accounted for properly in the calculation of the  $\text{H}_2\text{O}$  photodissociation rate.
- (2) The effects of eddy transport are taken into account by a numerical integration technique.

(3) A physically acceptable eddy diffusion coefficient is used that falls within the upper and lower bounds determined respectively by (a) an empirical upper limit on the OH density and (b) a consideration of the total available water vapor at 35 km coupled with indirectly observed phenomena requiring an  $H_2O$  mixing ratio of approximately 1 part per million at 85 kilometers.

The upper boundary of the model was chosen to be 85 km because the lifetime of atomic hydrogen becomes longer than the characteristic diffusion time near this altitude.

Diurnal variations of OH are not treated in the calculations because the launch took place about 10 minutes before solar illumination left the lower portion of the layer (65 km) under consideration. Of course the termination of ozone photolysis (which indirectly controls the OH density), occurs before the solar flux is extinguished in a given layer at 3100 Å because of the enlarged optical depth at the peak of the  $O_3$  Hartley bands at 2550 Å. High time resolution studies by Park and London (1970) indicate OH volume density enhancements at 65 km of about 40 percent above daytime values at the time the experiment was carried out. However, the enhancement decreases quite rapidly with altitude so the column density considerations upon which the conclusions are based are not significantly affected. Also, the changes in hydroxyl density during the nonequilibrium twilight period are a sensitive function of the rate constants chosen for the reactions used in the time integration, making quantitative conclusions very difficult.

A final note in criticism concerns the assumption of a constant eddy diffusion coefficient. This assumption is most certainly incorrect but at the present time the diffusion coefficient represents an undetermined problem experimentally as well as theoretically. Although numerous mechanisms have been proposed that would provide the eddy motion, the diurnal, altitude and latitude dependence of the resulting eddies is unknown. The alternative approach adopted here is to formulate the problem in terms of a parameter called the "diffusion coefficient." It is also worth noting that the interpretation of the experimental results depends most critically upon the diffusion coefficient between 50 and 65 kilometers which is a region sufficiently narrow to diminish largely the altitude dependence of the diffusion coefficient.

## SUMMARY AND CONCLUSIONS

A Nike-Apache rocket was launched into the mesosphere under twilight conditions to study the ultraviolet resonance fluorescence of the hydroxyl molecule with a scanning spectrometer. An upper limit on the column density of OH is established throughout the region between 65 and 85 kilometers. An analysis of the characteristic lifetimes of the reactive species  $H_2O$ , OH, H and  $HO_2$  allows the diffusing constituents to be treated in a physically meaningful manner without needlessly complicating the general solution.

The photodissociation rate for water vapor is calculated taking into account the critical column density dependence of the  $O_2$  effective cross section in the region of the Schumann-Runge band system. It is concluded that a significant amount of water vapor dissociation occurs down to the bottom of the mesosphere. This result, in conjunction with the eddy diffusion calculations, demonstrates that a water vapor mixing ratio on the order of 1 part per million at 80 km required by theories of noctilucent clouds and water vapor ions, requires an eddy diffusion coefficient equal to or larger than  $5 \times 10^5 \text{ cm}^2/\text{sec}$ . It is shown that in general, for a given  $H_2O$  mixing ratio at the mesopause, the larger dissociation rate at the stratopause places a significantly larger burden on the transport processes in the mesosphere.

The critical need for an accurate determination of the  $H_2O$  density at the mesopause is accentuated by the above conclusions because an empirically determined mixing ratio at 80 km of  $5 \times 10^{-8}$  or larger will provide important clues to the transport processes operating in the upper atmosphere.

The OH column density is demonstrated to be a direct func-

tion of the eddy diffusion coefficient and the experimental determination of the OH column density upper limit is shown to constrain the diffusion coefficient to values less than  $4 \times 10^6 \text{ cm}^2/\text{sec}$  in the lower mesosphere. Guided by these restrictions on the eddy diffusion coefficient, a model for mesospheric H<sub>2</sub>O, OH, H and HO<sub>2</sub> is presented using a diffusion coefficient of  $1 \times 10^6 \text{ cm}^2/\text{sec}$  and an H<sub>2</sub>O mixing ratio at 50 km of 5 parts per million.

#### ACKNOWLEDGMENTS

I wish particularly to thank Dr. Charles A. Barth for originally suggesting an examination of OH emission in the ultraviolet. His continued encouragement and support as my thesis advisor were essential in bringing this study to its present point.

I would like also to thank Dave Andrews and Gene Kadar of the Goddard Space Flight Center for their flawless instrumentation and vehicle support. Donald E. Anderson of the University of Colorado served as an able colleague in the calibration and field operation during the launch phase.

Financial support for my graduate studies came from the National Science Foundation, the Ford Foundation and the National Aeronautics and Space Administration.

## BIBLIOGRAPHY

- Anderson, J. G., and L. G. Meira, Jr., "Polarization of Rayleigh Scattered Radiation," L.A.S.P. Memorandum to C.A. Barth, 1969.
- Blake, A. J., J. H. Carver and G. N. Haddard, "Photo-Absorption Cross Sections of Molecular Oxygen Between 1250 Å and 2350 Å," J. Quant. Spect. Rad. Transfer, 6, 451, 1966.
- Brinkmann, R. T., A.E.S. Green and C. A. Barth, "Digitalized Solar Ultraviolet Spectrum," Jet Propulsion Laboratory Tech. Report No. 32-951, 1966.
- Brückner, G., "Photometrischer Atlas des Nahen Ultravioletten Sonnenspektrums, 2988 Å - 3629 Å, Gottengen, Germany, Vandenhoeck and Ruprecht, 1960.
- Bruner, E. C., and W. A. Rense, "Rocket Observations of Profiles of Solar Ultraviolet Emission Lines," Ap. J. 157, 417, 1969.
- Campbell, I. M. and B. A. Thrush, "The Association of Oxygen Atoms and Their Combination with Nitrogen Atoms," Proc. Roy. Soc., A, 296, 222, 1967.
- Chapman, S. and P. C. Kendall, "Noctilucent Clouds and Thermo-spheric Dust: The Diffusion and Height Distribution," Quart. J. Roy. Met. Soc., 91, 115, 1965.
- CIRA 1965, Cospar International Reference Atmosphere 1965, North-Holland Publishers Company, Amsterdam, 1965.
- Clyne, M.A.A., and B. A. Thrush, "Rates of Elementary Processes in the Chain Reactions Between Hydrogen and Oxygen, 2, Kinetics of the Reaction of Hydrogen Atoms with Molecular Oxygen," Proc. Roy. Soc. London, A, 275, 559, 1963.
- Demore, W. B., "Reaction of O(<sup>1</sup>D) with H<sub>2</sub> and the Reactions of H and OH with Ozone," J. Chem. Phys., 37, 2048, 1962.
- Ditchburn, R. W. and P. A. Young, "The absorption of Molecular Oxygen Between 1850 and 2500 Å," J. Atmos. Terr. Phys., 24, 127, 1962.

BIBLIOGRAPHY (continued)

Fastie, W. G., "A Small Plane Grating Monochromator," J. Opt. Soc. Am., 42, 641, 1952.

Ferguson, E. E., Private communication, 1970.

Foner, S. N. and R. L. Hudson, "Mass Spectrometry of the HO<sub>2</sub> Free Radical," J. Chem. Phys., 36, 2681, 1962.

Furukawa, P. M., P. C. Haagenson, M. J. Scharberg, "A Composite, High Resolution Solar Spectrum from 2080 to 3600 Å," NCAR-TN-26, 1967.

Golden, D. M., F. P. Del Greco and F. Kaufman, "Experimental Oscillator Strength of OH,  $^2\Sigma - ^2\pi$  by a Chemical Method," J. Chem. Phys., 39, 3034, 1963.

Goody, R. M., Atmospheric Radiation I - Theoretical Basis, Oxford University Press, London, 1964.

Hesstvedt, E., "On the Effect of Vertical Eddy Transport on Atmospheric Composition in the Mesosphere and Lower Thermosphere," Geophys. Publik. Geophys. Norvegica, 27, 1, 1968.

Hinteregger, H. E., L. A. Hall, and G. Schmidtke, "Solar XUV Radiation and Neutral Particle Distribution in the July 1963 Thermosphere," Space Res., 5, 1175, 1965.

Hudson, R.D., V. L. Carter and F. L. Breig, "Predissociation in the Schumann-Runge Band System of O<sub>2</sub>: Laboratory Measurements and Atmospheric Effects," J. Geophys. Res., 74, 4079, 1969.

Hudson, R. D., Private communication, 1970.

Hunt, B. G., "Ozone's Photochemistry in Moist Atmosphere," J. Geophys. Res., 71, 1385, 1966.

Inn, E. C. Y., and Y. Tanaka, "Absorption Coefficients of Ozone in the Ultraviolet and Visible Region," J. Opt. Soc. America, 43, 870-873, 1953.

Kaufman, R. and J. R. Kelso, "Rate Constant of the Reaction  $O + 2O_2 \rightarrow O_3 + O_2$ ," *Discussions Faraday Soc.*, 37, 26, 1964.

Kaufman, F., "Aeronomic Reactions Involving Hydrogen, A review of Recent Laboratory Studies," *Am. Geophys.*, 20, 106-114, 1964.

Krueger, A. J., and W. R. McBride, "Sounding Rocket - OGO-IV Satellite Ozone Experiment: Rocket Ozonesonde Measurements," Naval Weapons Center TP#4667, 1968.

Mastenbrook, H. J., "Water Vapor Distribution in the Stratosphere and High Troposphere," *J. Atm. Sci.*, 25, 299, 1968..

McCalla, T. R., Introduction to Numerical Methods and Fortran Programming, John Wiley and Sons, 1967.

Meinel, A. B., "OH Emission Bands in the Spectrum of the Night Sky," *Astrophys. J.*, 111, 555, 1950.

Narcisi, R. S., and A. D. Bailey, "Mass Spectrometric Measurements of Positive Ions at Altitudes from 64 to 112 Kilometers," *J. Geophys. Res.*, 70, 3687, 1965.

Narcisi, R. S., "On Water Cluster Ions in the Ionospheric D-Region," *Space Res.*, 9, 560, 1969.

Nicolet, M., "Introduction of Chemical Aeronomy, "Discussions of the Faraday Society, 32, 21, 1964.

Nicolet, M., "Ozone and Hydrogen Reactions", *Aeronomica Acta A - N° 70 - 1970*.

Packer, D. M., "Altitudes of the Night Airglow Radiations, "Ann. de Geophys., 17, 67, 1961.

Park, J. and J. London, Private communication, 1969.

Park, J. and J. London, Private communication, 1970.

Schiff, H. I., "Neutral Reactions Involving Oxygen and Nitrogen," *Can. J. Chem.*, 47, 1903, 1969.

Schofield, K., "An Evaluation of Kinetic Rate Data for Reactions of Neutrals of Atmospheric Interest," *Planet. Space Sci.*, 15, 643, 1967.

Shimazaki, T., Private communication, 1969.

Slanger, T. G., G. Black and R. A. Young, 8th Informal Conference on Photochemistry, Ottawa, 1968.

BIBLIOGRAPHY (continued)

- Snelling, R. D. and E. J. Bain, "Deactivation of O(<sup>1</sup>D) by Molecular Oxygen," J. Chem. Phys., 48, 5737, 1968.
- Tanaka, Y., "Absorption Spectrum of Nitrogen in the Region from 1075 to 1650 Å," J. Opt. Soc. Amer., 45, 663, 1955.
- Tarasova, T. M., "Direct Measurements of the Night Airglow in the Spectral Region  $\lambda = 8650 \text{ Å}$ ," Planetary Space Sci., 11, 437, 1963.
- Thompson, B. A., P. Harteck and R. R. Reeves, Jr., "Ultraviolet Absorption Coefficient of CO<sub>2</sub>, CO, O<sub>2</sub>, H<sub>2</sub>O, N<sub>2</sub>O, NH<sub>3</sub>, NO, SO<sub>2</sub> and CH<sub>4</sub> Between 1850 and 4000 Å," J. Geophys. Res. 68, 6431, 1963.
- U. S. Standard Atmosphere Supplements, 1966, U.S. Government Printing Office, Washington, D. C. 20402.
- Watanabe, K., Advances in Geophysics, Vol. V, Academic Press, New York, 1958.
- Westenberg, A. A. and N. De Haas, "Quantitative ESR Measurements of Gas-Phase H and OH Concentrations in the H-NO<sub>2</sub> Reactions," J. Chem. Phys., 43, 1550, 1965.
- Witt, G., "The Nature of Noctilucent Clouds," Space Research IX, 157, 1969.

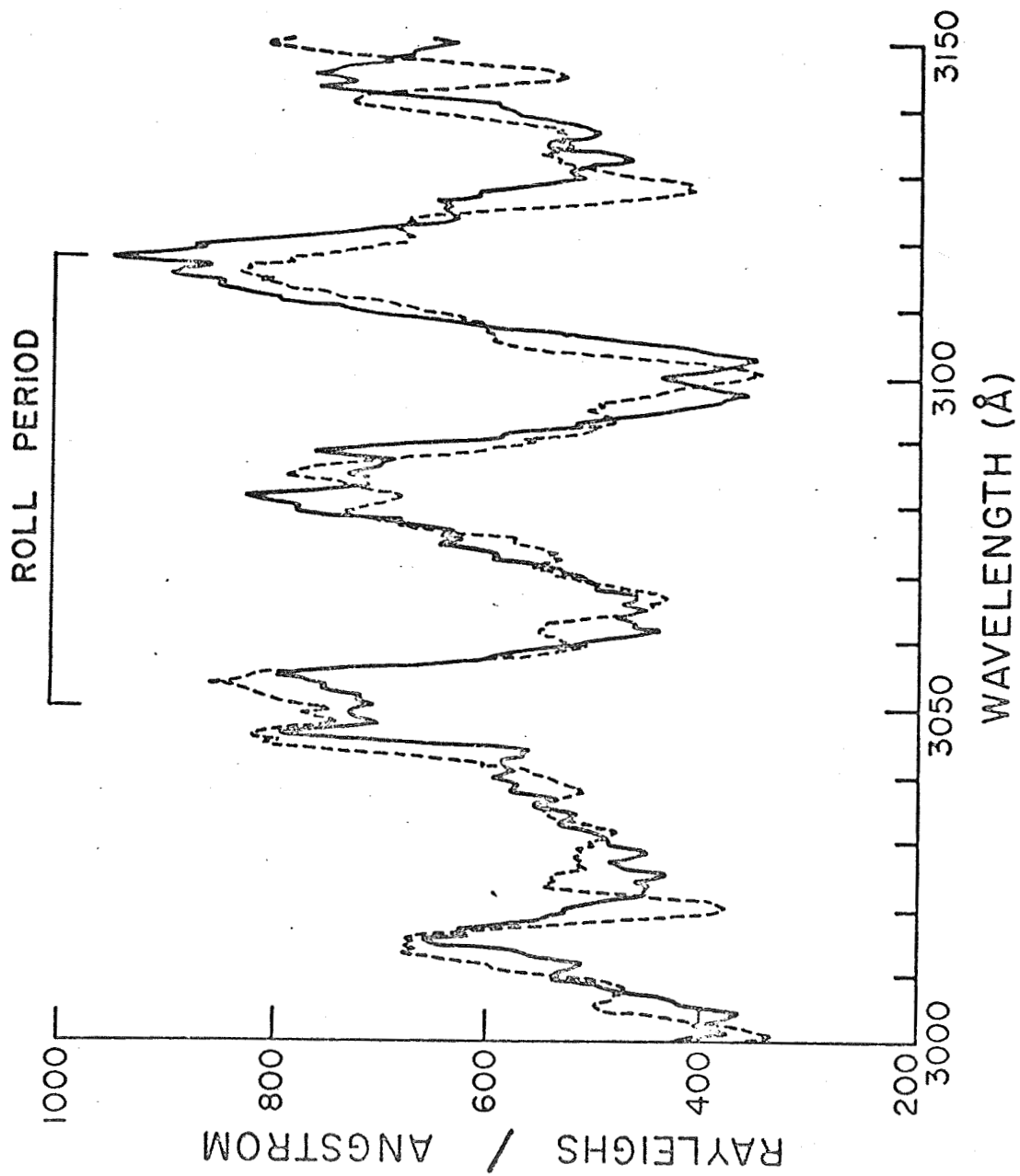


Fig. 1 Comparison of Rocket Data to Background Constructed Using Spectrographically Measured Solar Flux. The Dotted Line Indicates the Constructed Background with the Roll Period Indicated by the Bracket. Altitude: 69 km.

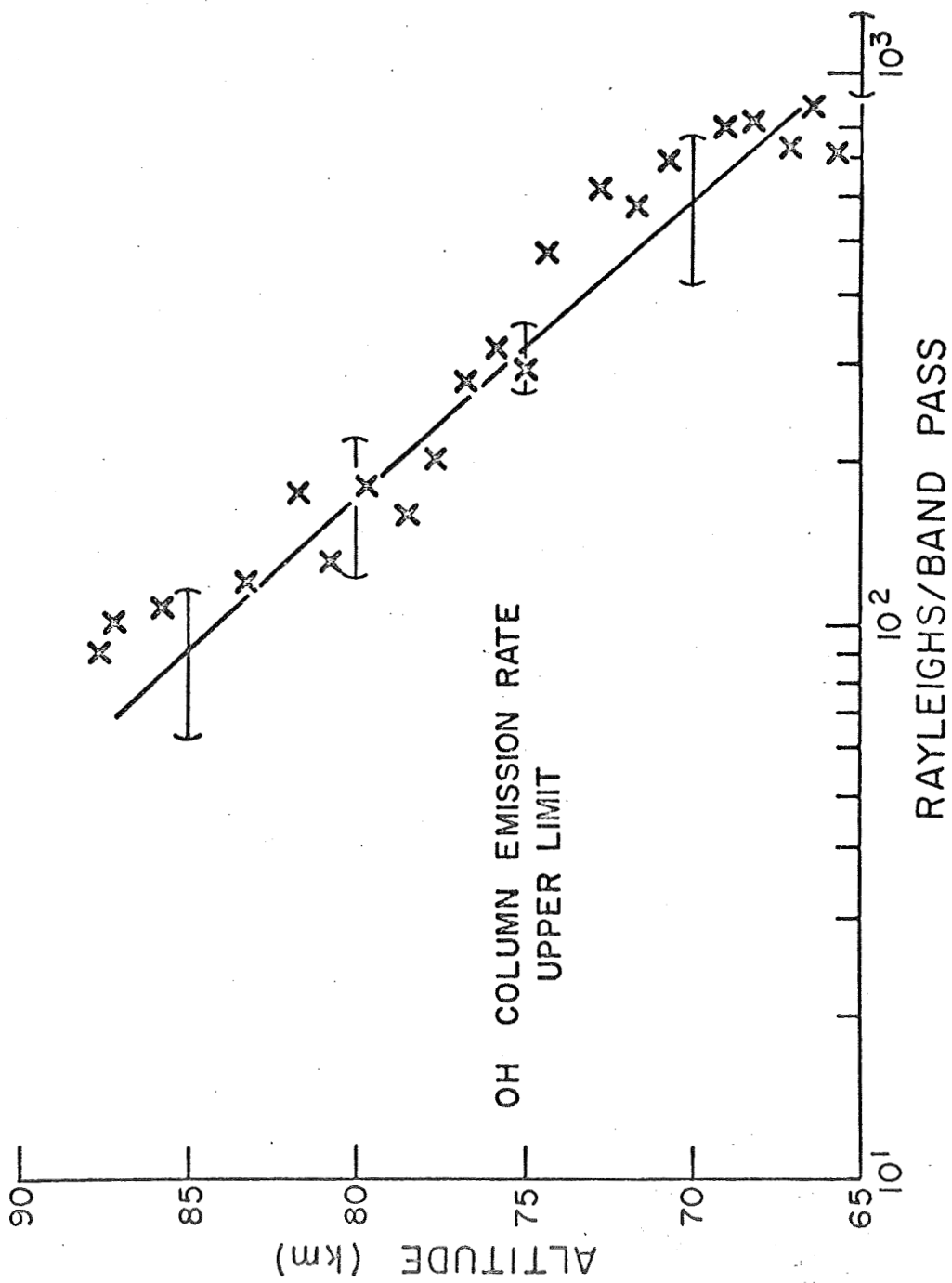


Fig. 2 Hydroxyl Column Emission Rate Upper Limit Between 65 and 85 km.

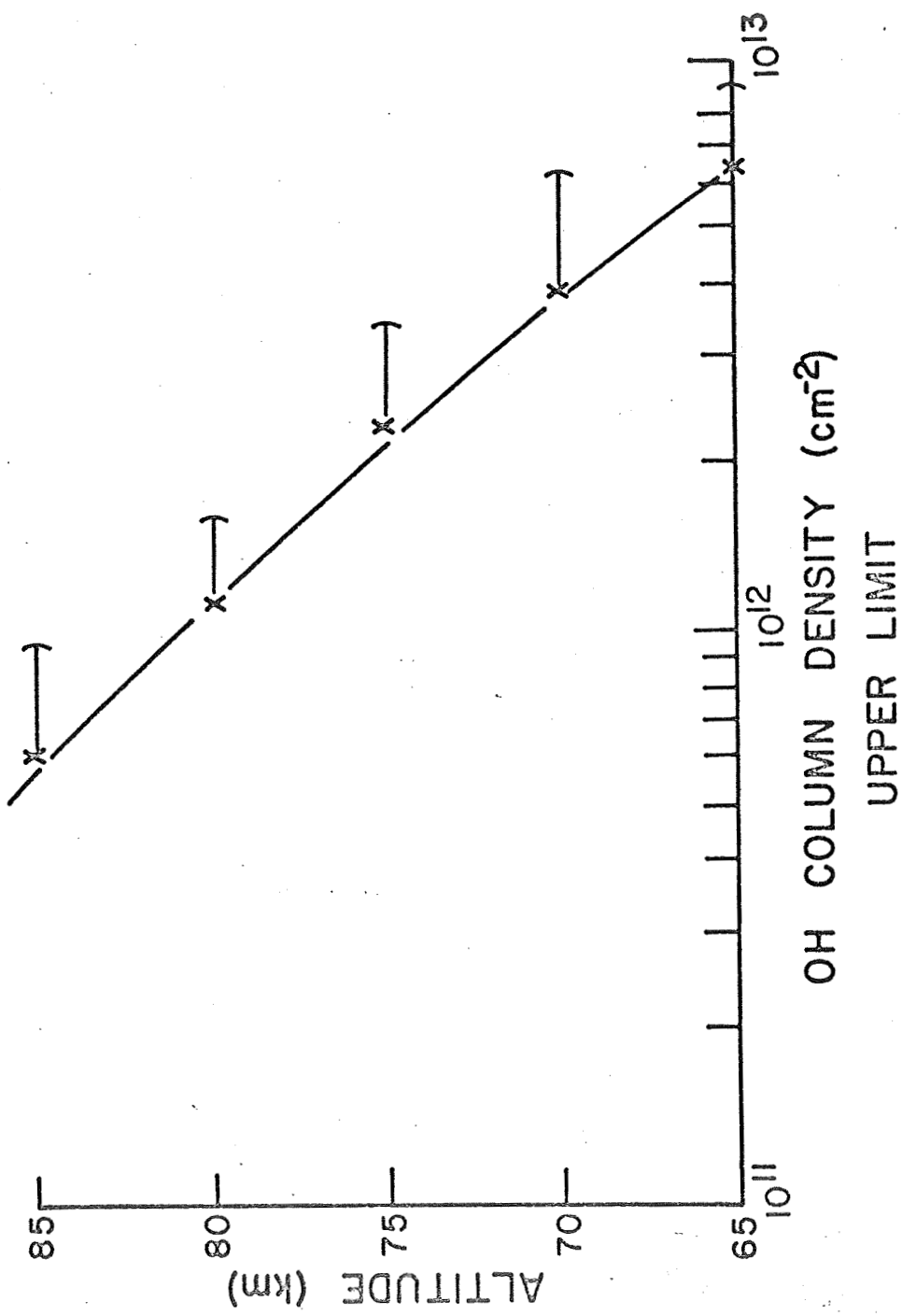


Fig. 3 Hydroxyl Column Density Upper Limit Between 65 and 85 km.

## ABSORPTION CROSS SECTION OF $O_2$ AND $H_2O$

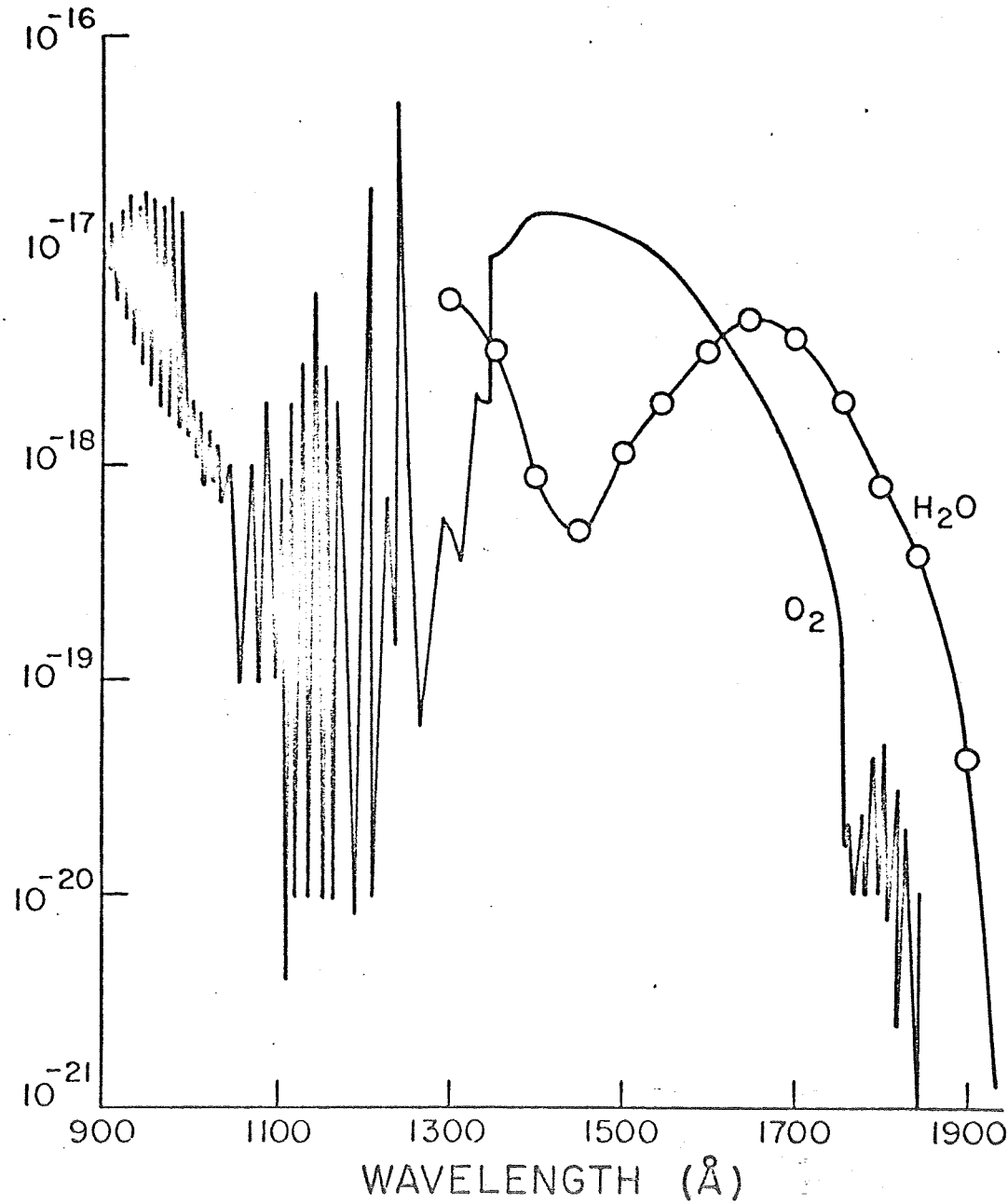


Fig. 4 Schematic of the Absorption Cross Sections for  $H_2O$  and  $O_2$  (Watanabe, 1958).

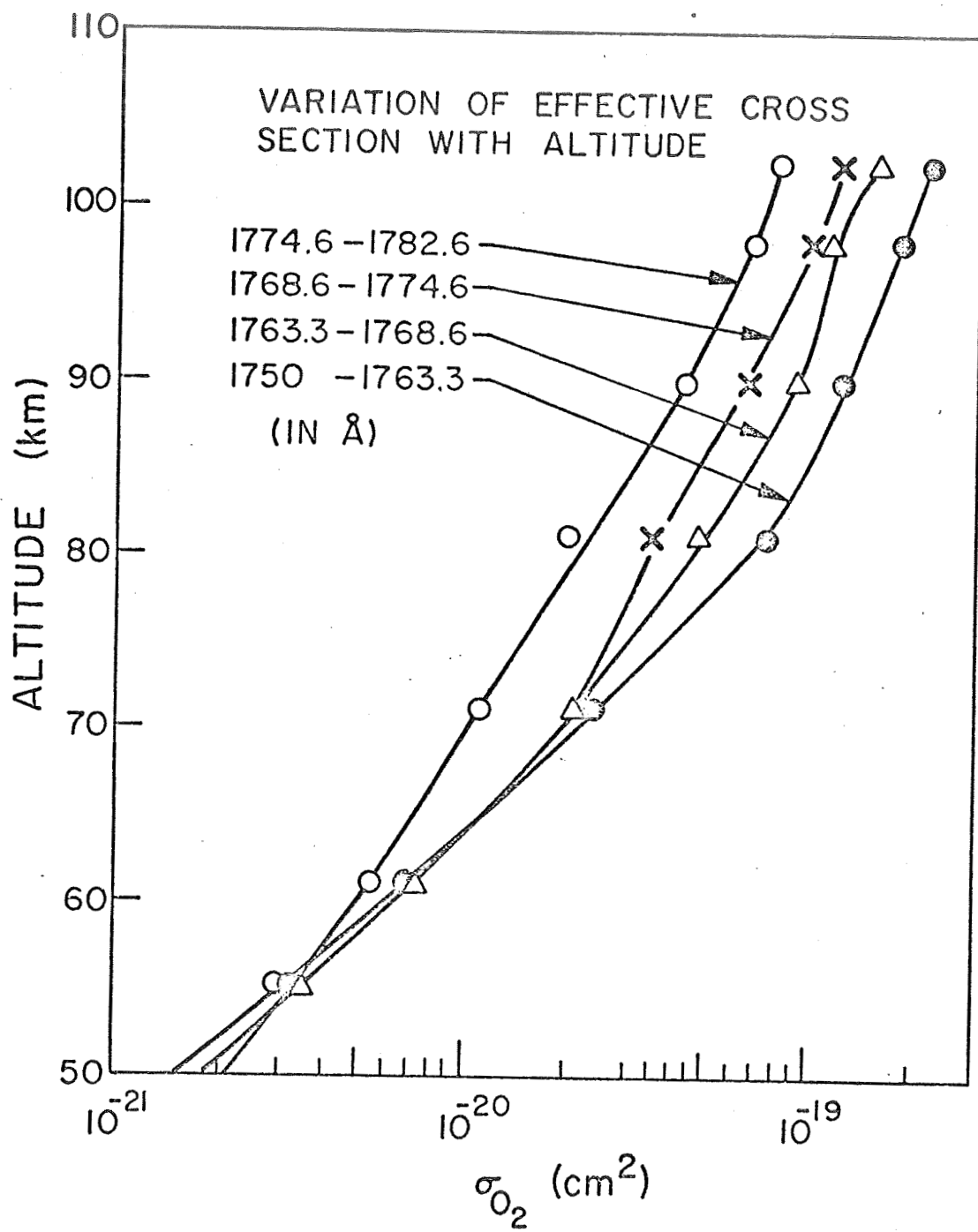


Fig. 5 The Effective Cross Section of  $O_2$  as a Function of Altitude in the Earth's Atmosphere Determined in the Laboratory by Hudson et al. (1969) for Four Wavelength Intervals Between 1750 and 1782.6 Å.

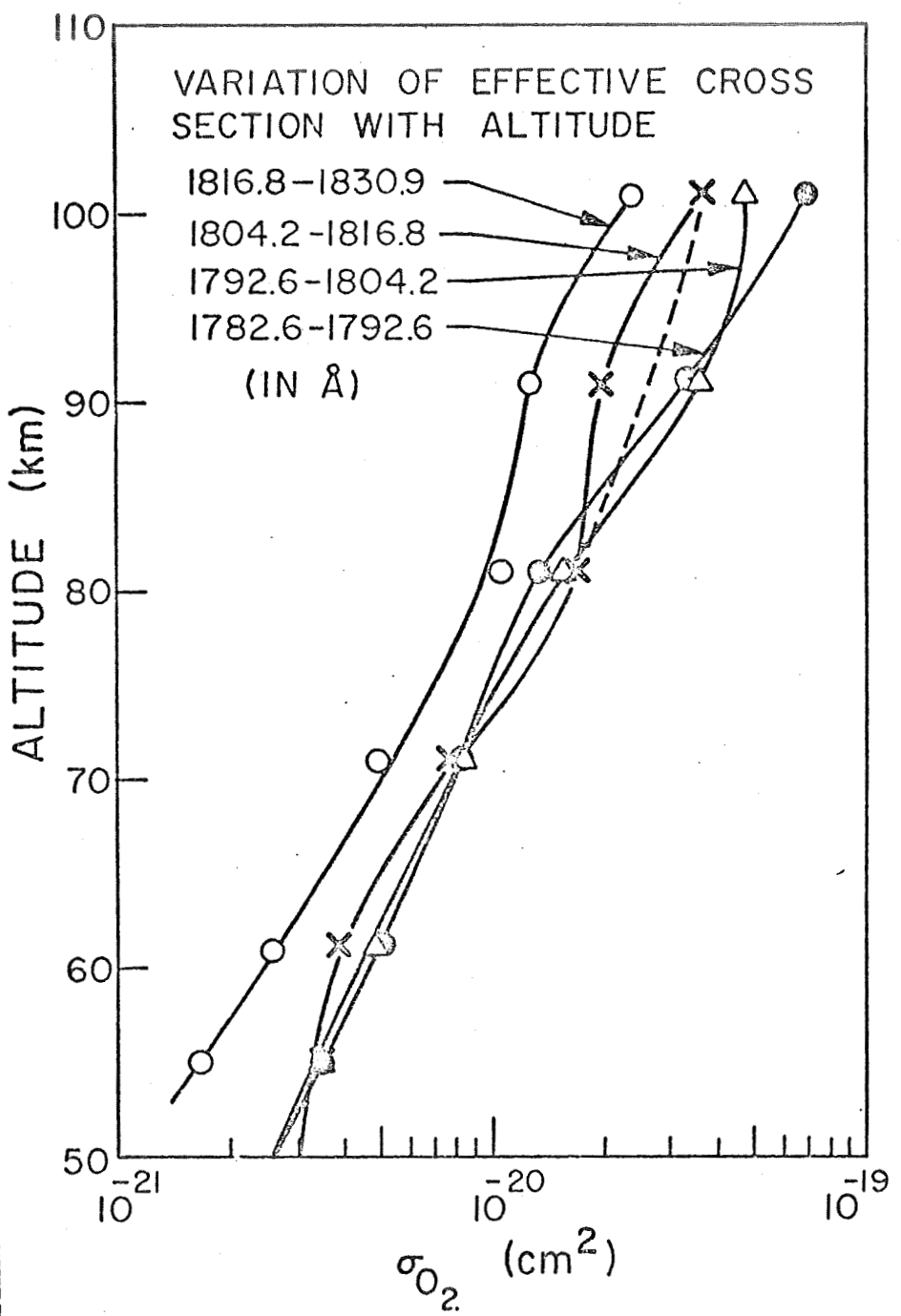


Fig. 6 The Effective Cross Section of  $O_2$  as a Function of Altitude in the Earth's Atmosphere Determined in the Laboratory by Hudson et al. (1969) for Four Wavelength Intervals Between 1782.6 and 1830.9 Å.

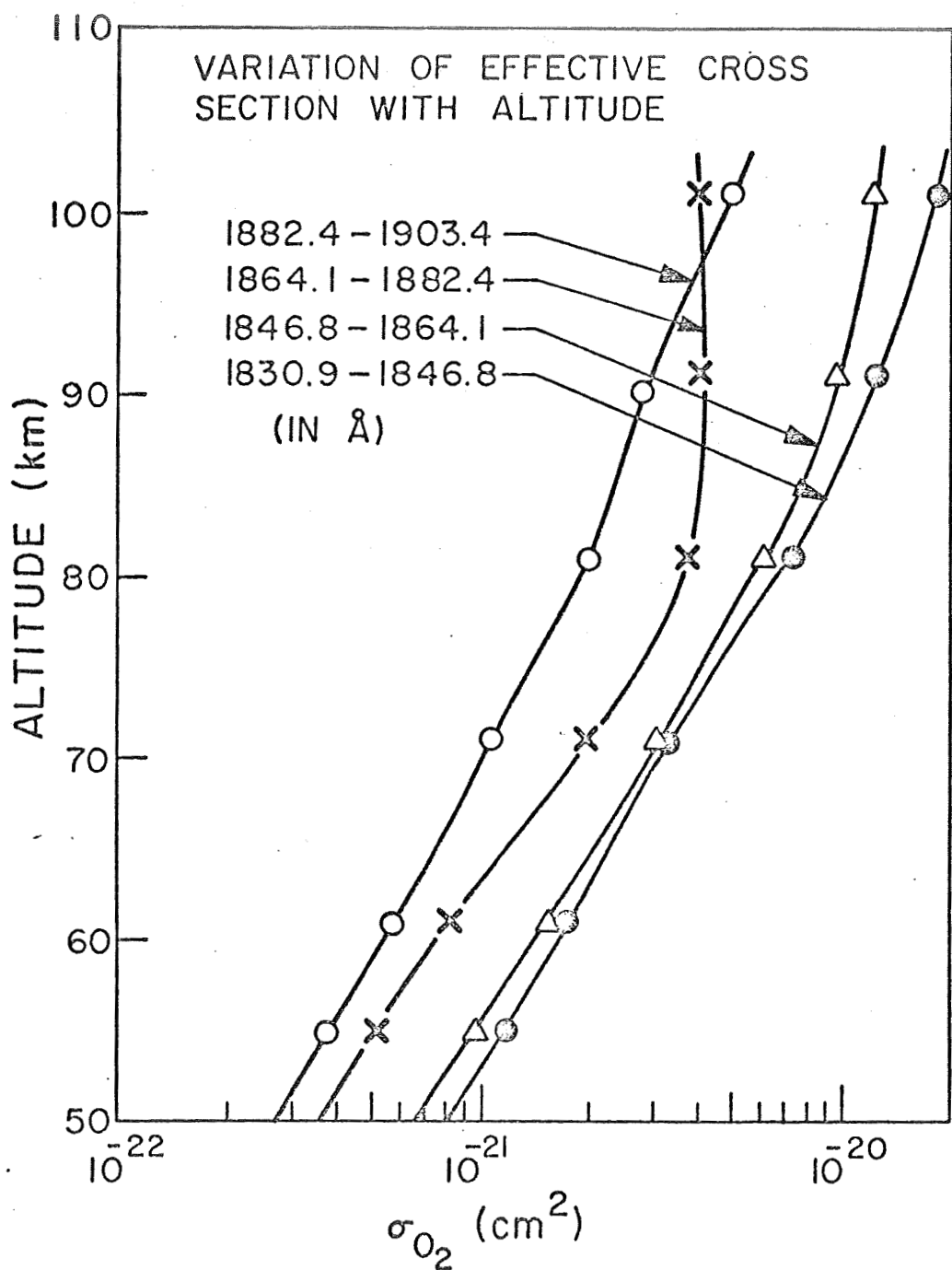


Fig. 7 The Effective Cross Section of  $O_2$  as a Function of Altitude in the Earth's Atmosphere Determined in the Laboratory by Hudson et al. (1969) for Four Wavelength Intervals Between 1830.9 and 1903.4 Å.

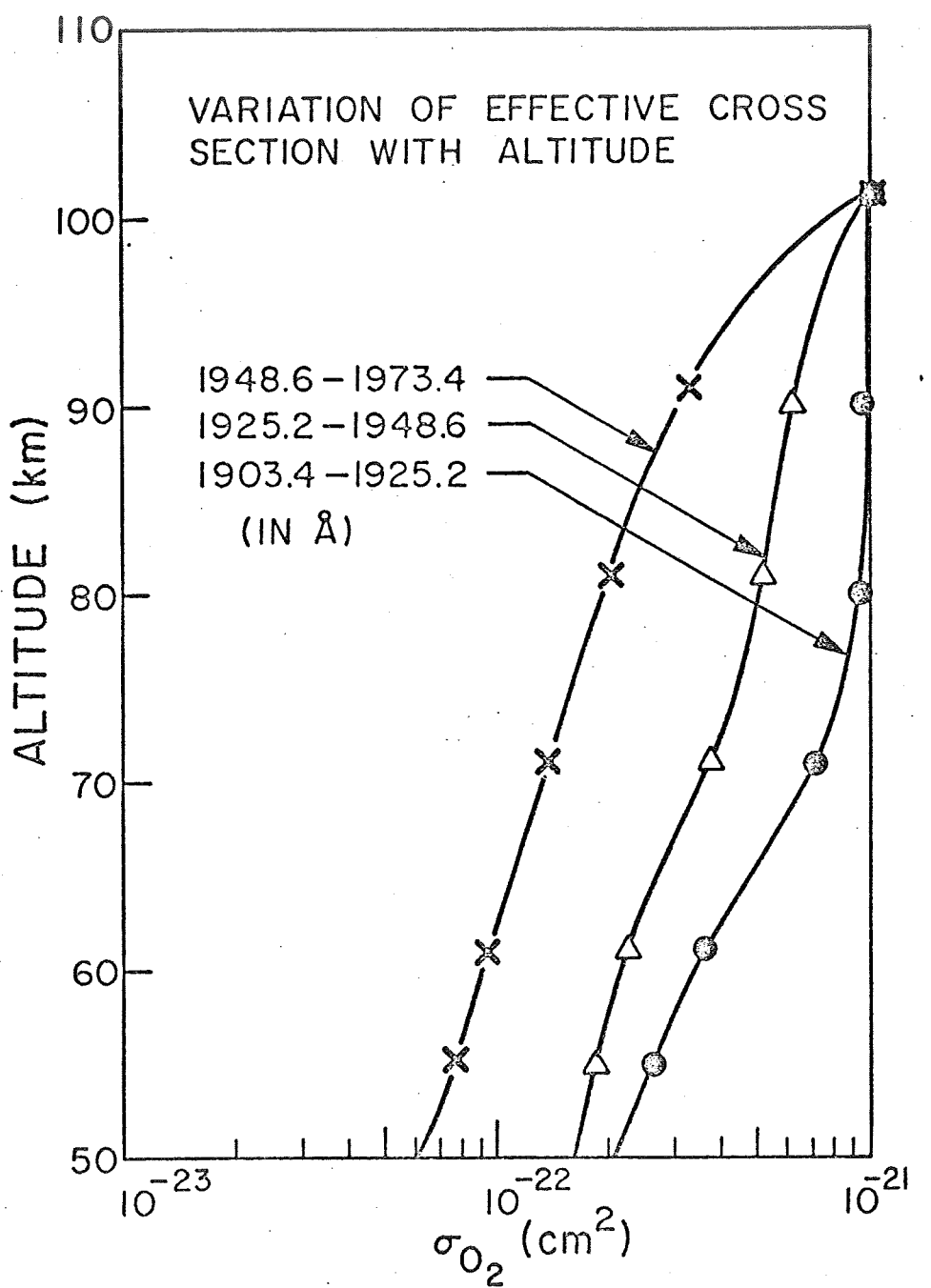


Fig. 8 The Effective Cross Section of  $O_2$  as a Function of Altitude in the Earth's Atmosphere Determined in the Laboratory by Hudson et al. (1969) for Three Wavelength Intervals Between 1903.4 and 1973.4 Å.

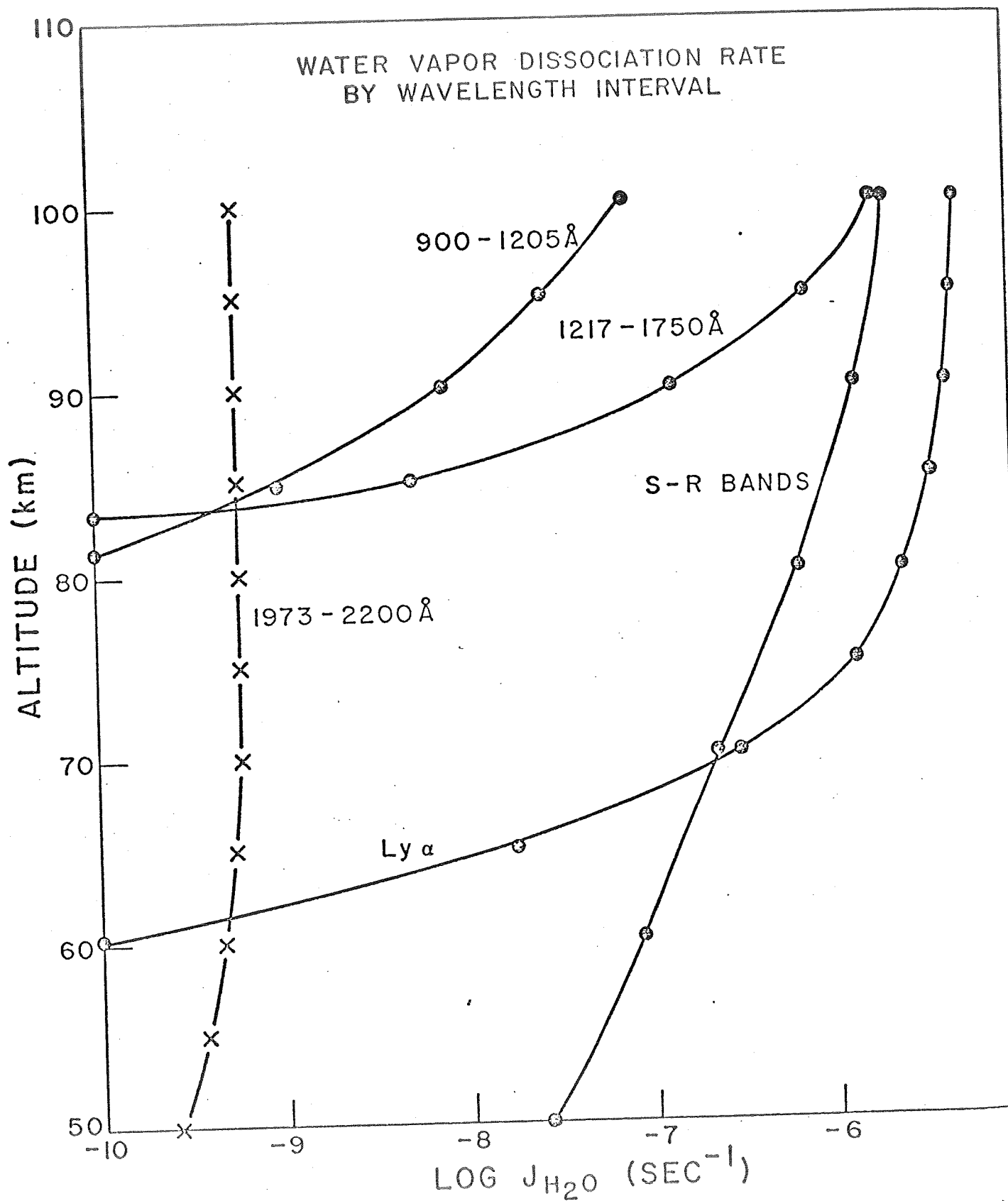


Fig. 9

Dissociation rate of water vapor for five separate spectral regions.

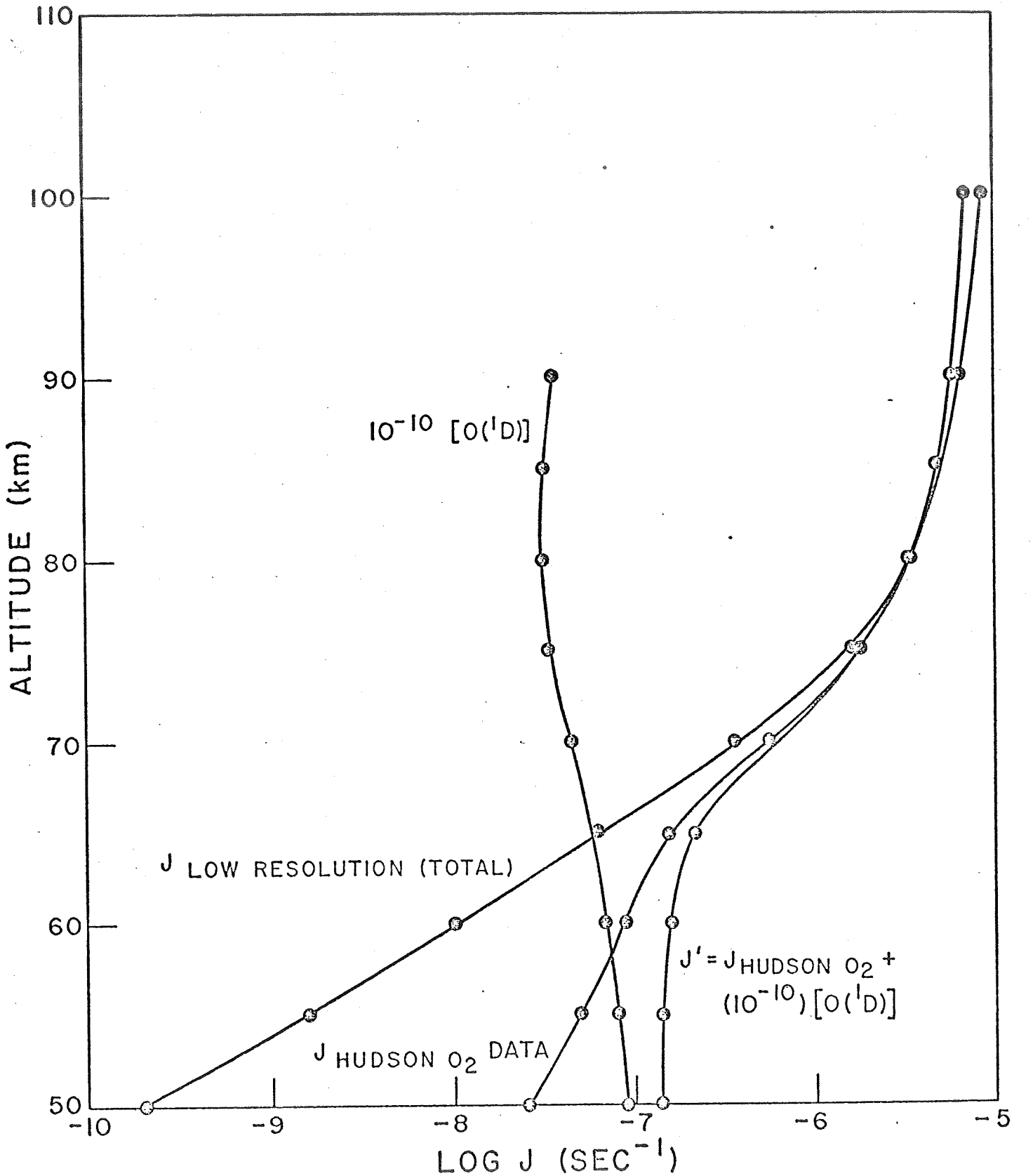


Fig. 10

Water vapor photodissociation rate from Figure 9 summed, compared to the dissociation rate using a low resolution survey in the Schumann-Runge Band System. Also displayed is the loss coefficient resulting from the reaction between  $O(^1D)$  and water vapor.

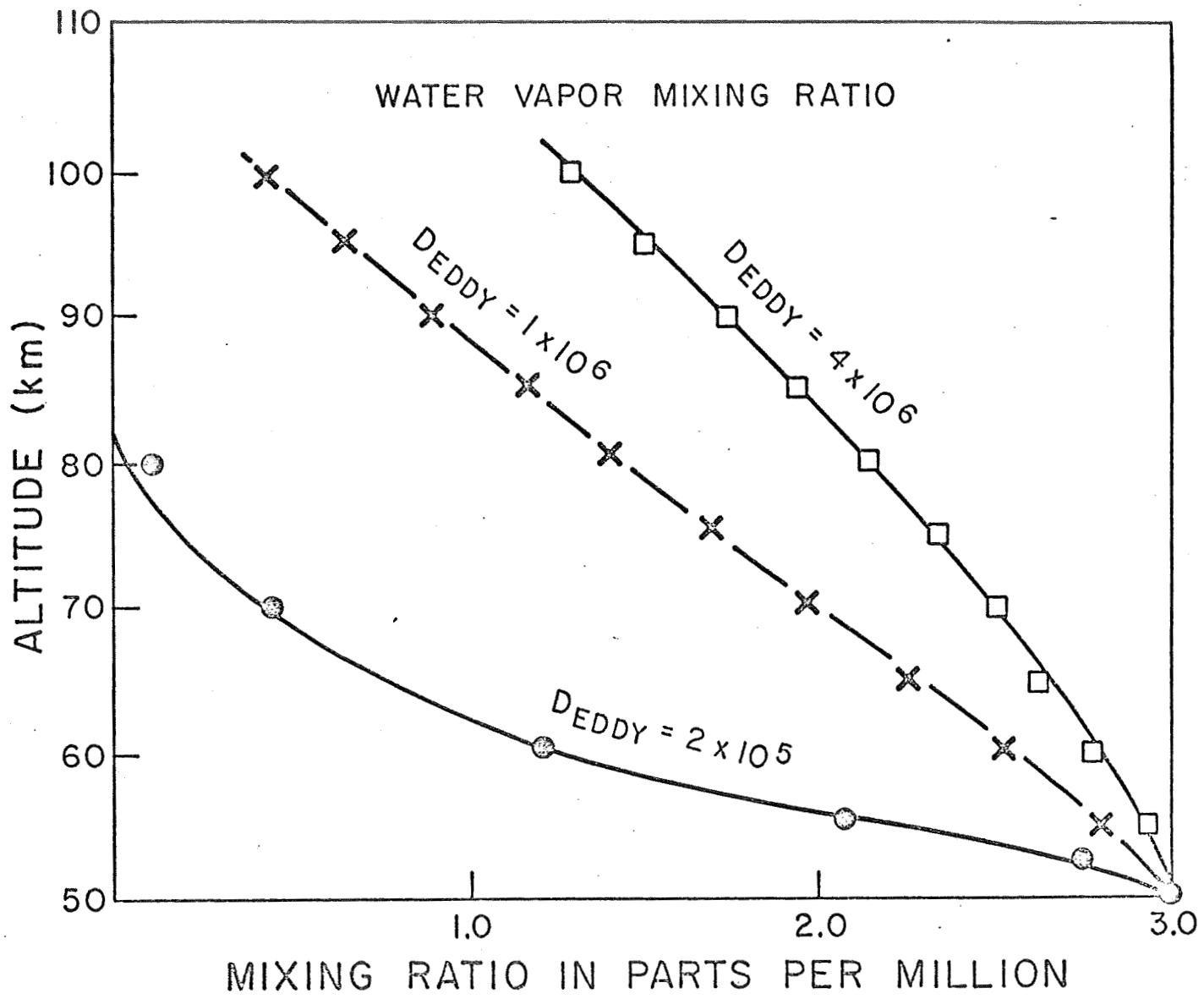


Fig. 11 Diffusion Solution for  $H_2O$  Using a Mixing Ratio of  $3 \times 10^{-6}$  at 50 km.

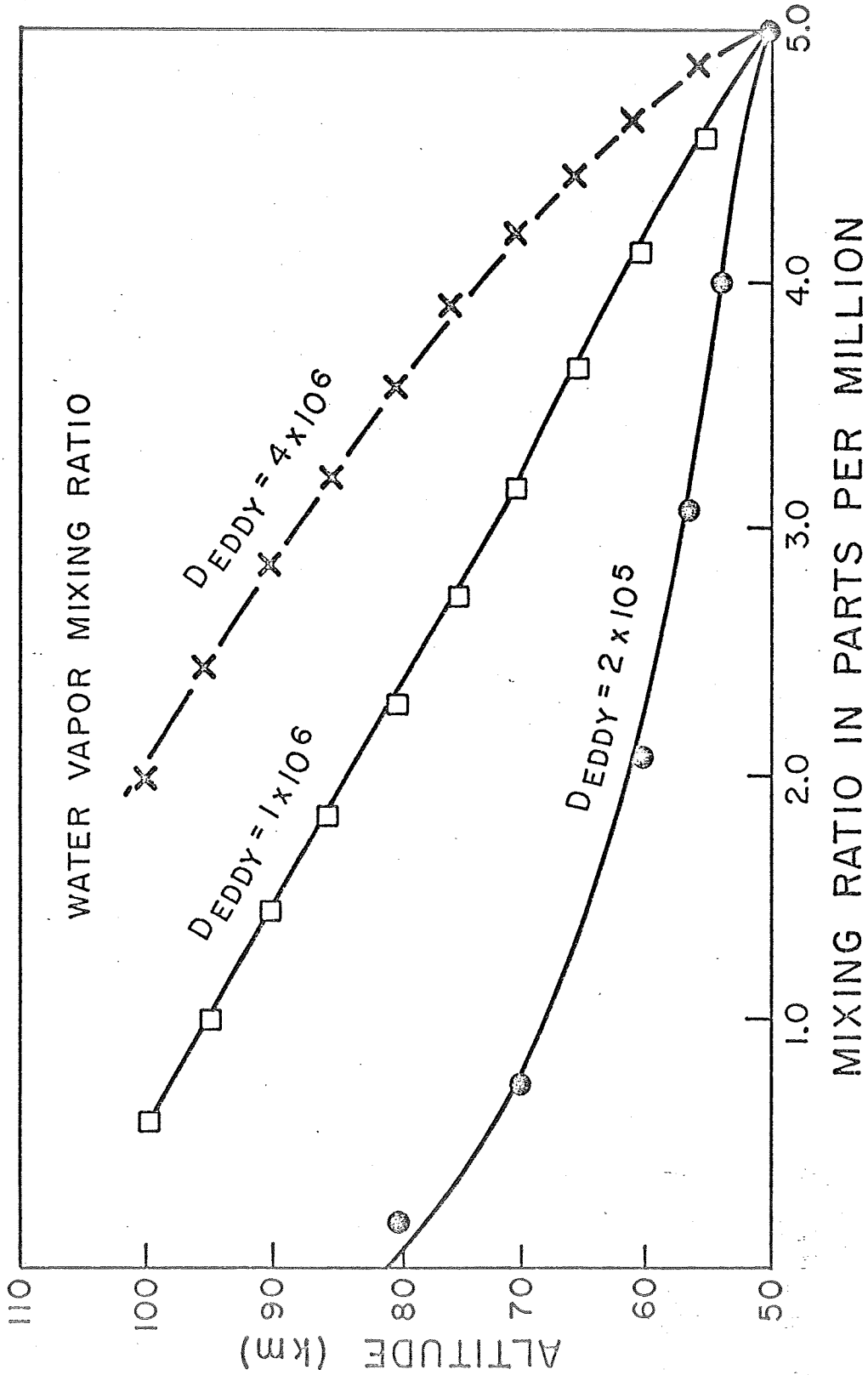


Fig. 12 Diffusion Solution for  $H_2O$  Using a Mixing Ratio of  $5 \times 10^{-6}$  at 50 km.

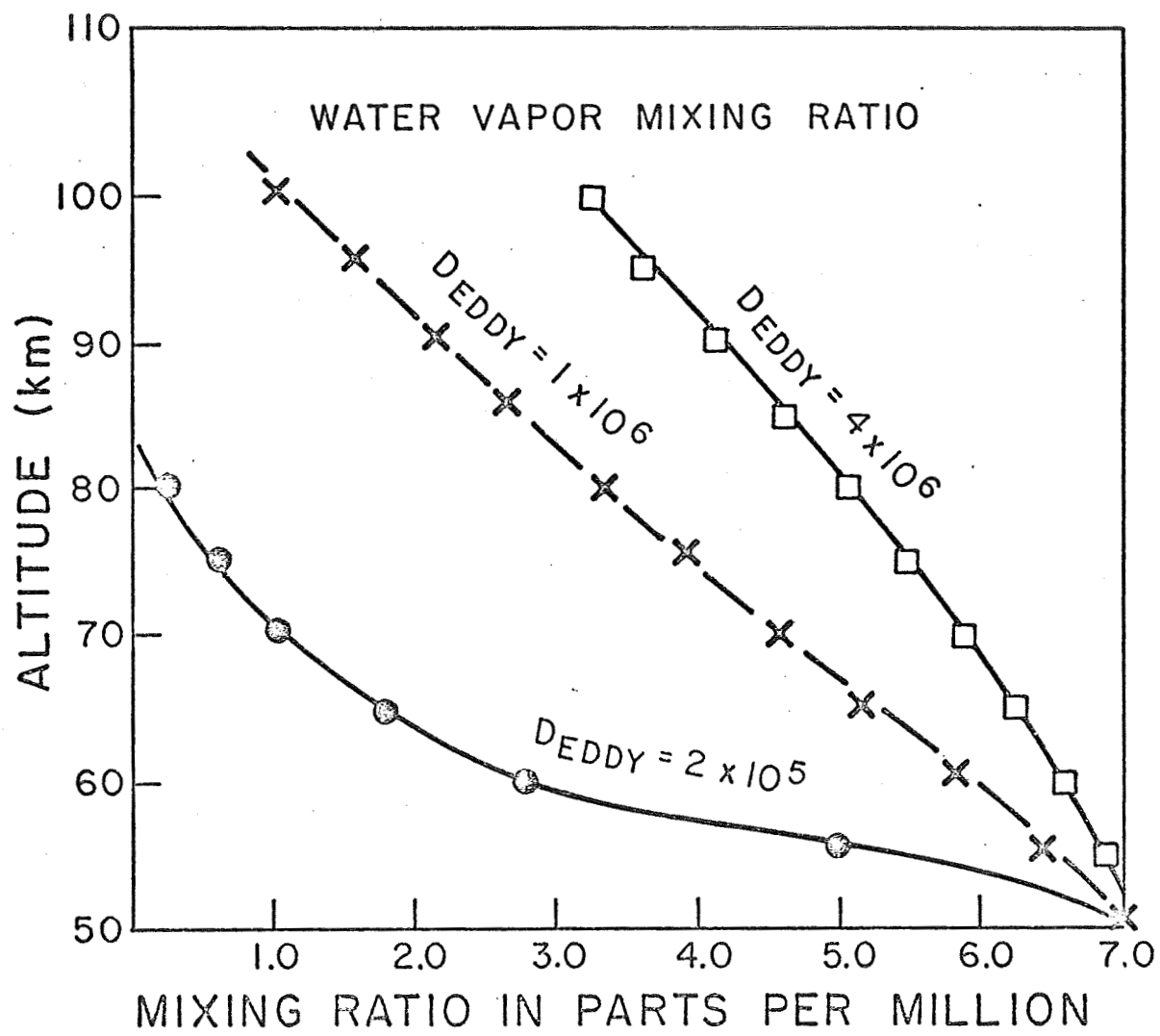


Fig. 13 Diffusion Solution for  $\text{H}_2\text{O}$  Using a Mixing Ratio of  $7 \times 10^{-6}$  at 50 km.

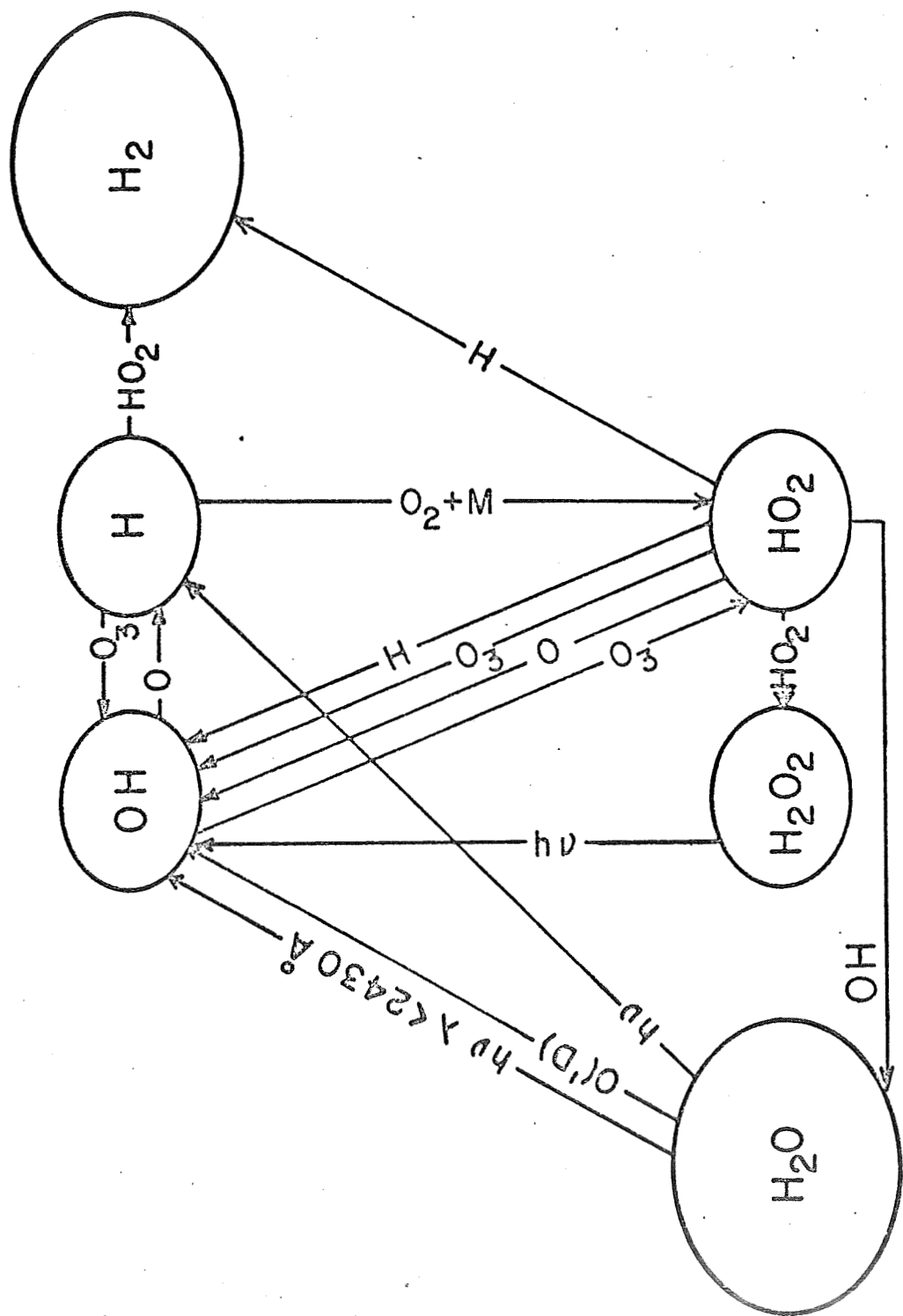


Fig. 14 Schematic of the Hydrogen Reaction Scheme

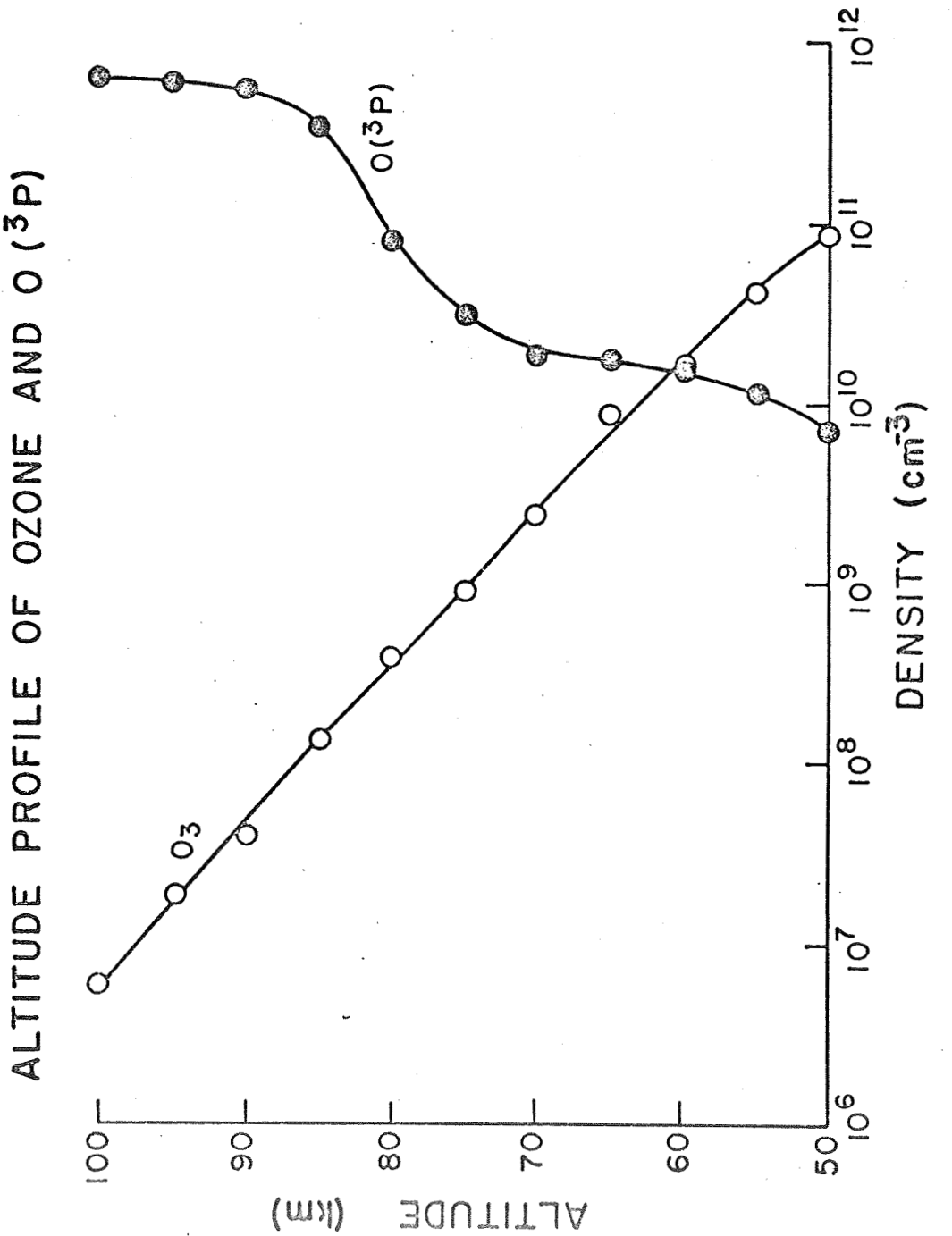


Fig. 15 Volume Density Profiles of Ozone and O(<sup>3</sup>P) (Park and London, 1969).

90

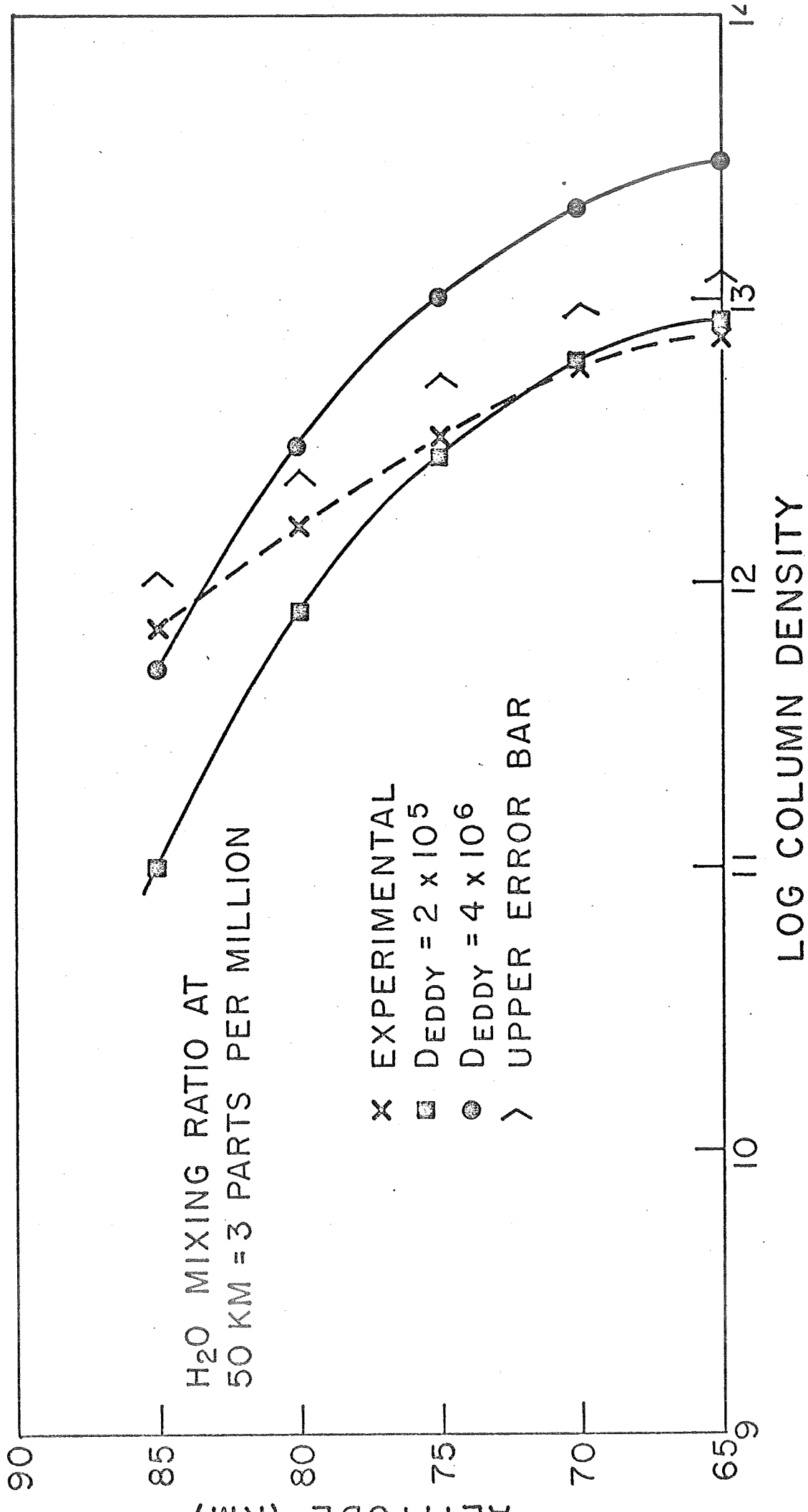


Fig. 16 Comparison of the Experimentally Determined Upper Limit to the Integrated Theoretically Determined Profiles of OH for a Water Vapor Mixing Ratio of  $3 \times 10^{-6}$  at 50 km.

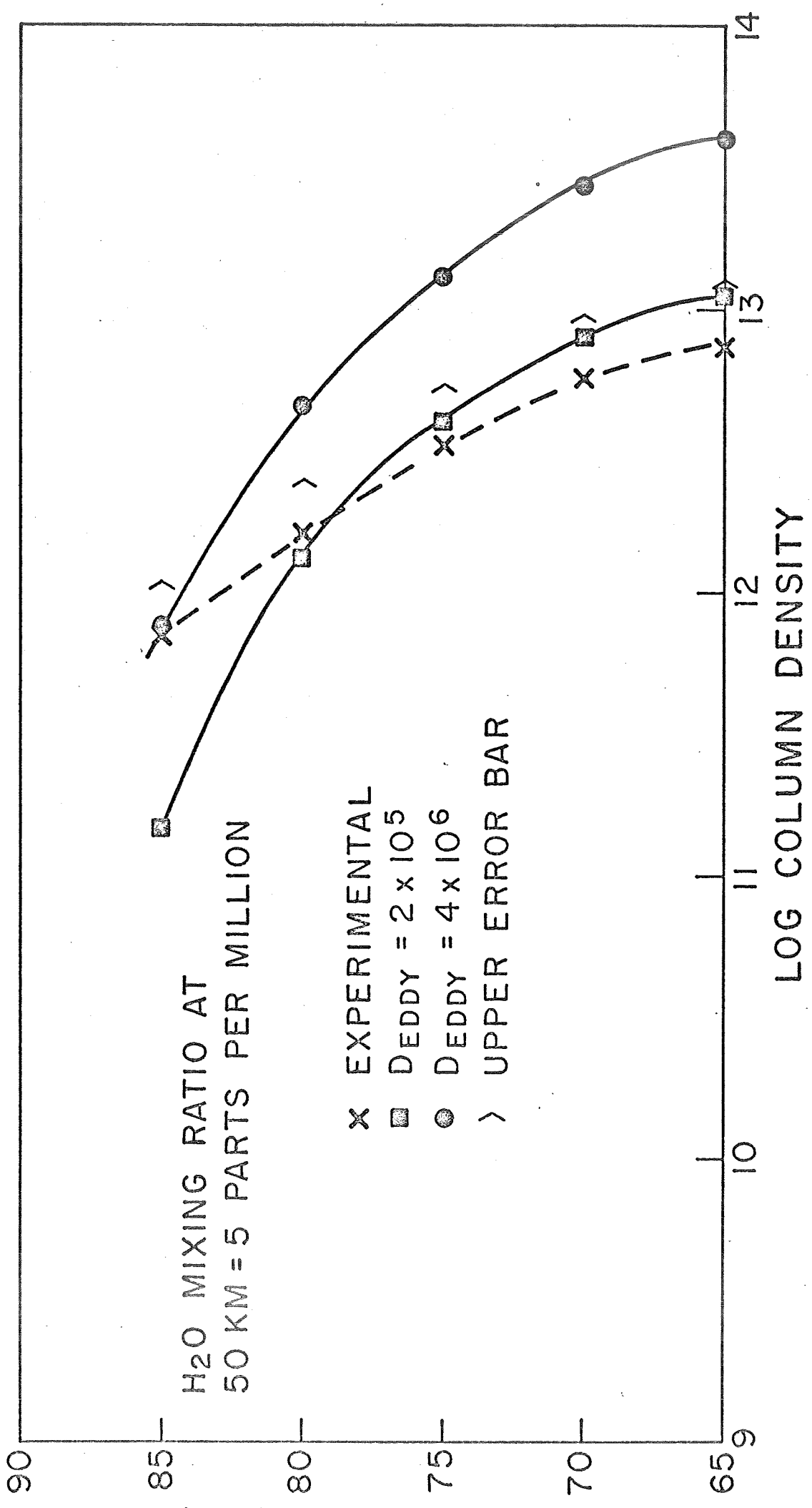


Fig. 17 Comparison of the Experimentally Determined Upper Limit to the Integrated Theoretically Determined Profiles of OH for a water Vapor Mixing Ratio of  $5 \times 10^{-6}$  at 50 km.

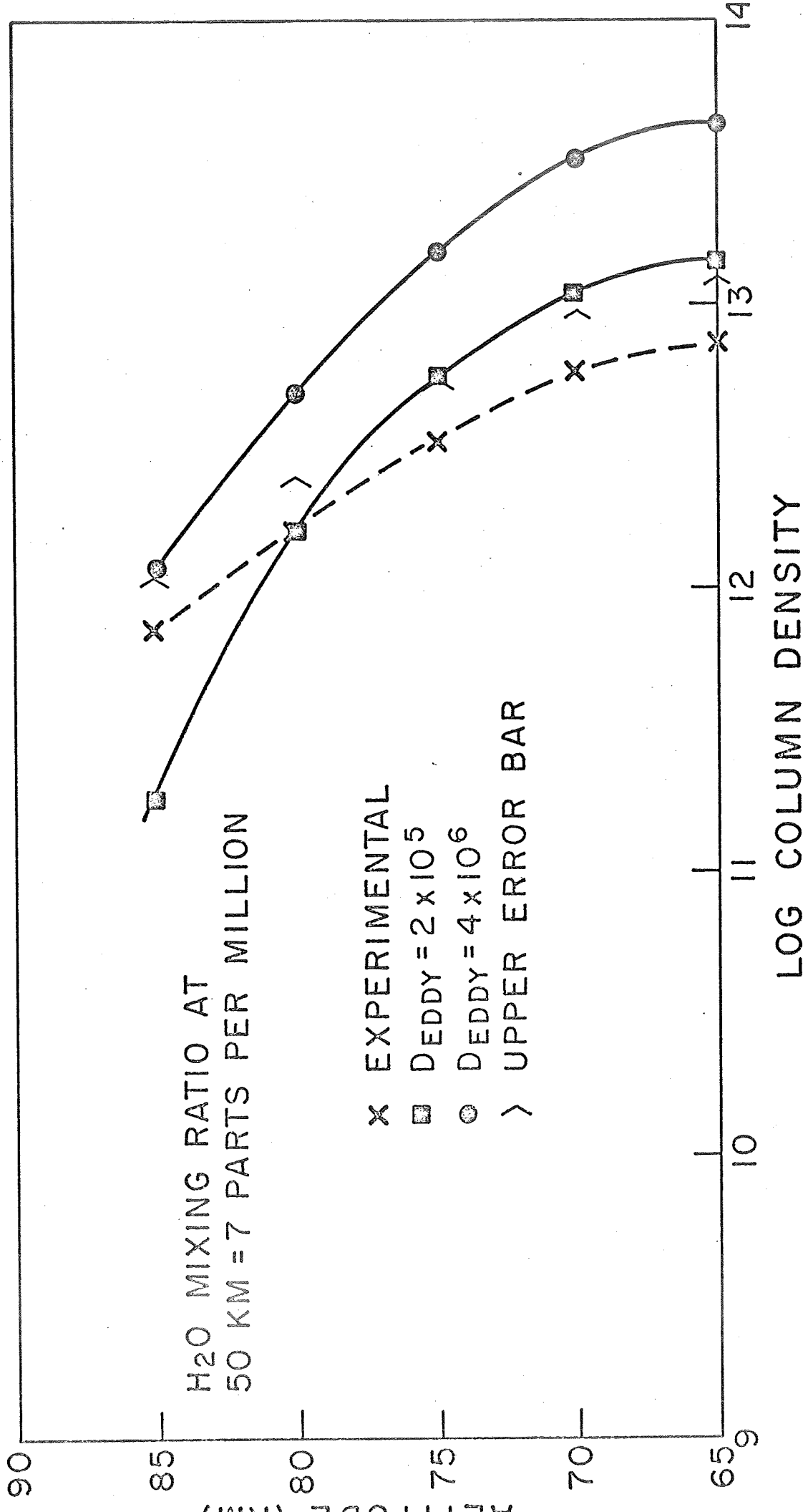


Fig. 18 Comparison of the Experimentally Determined Upper Limit to the Integrated Theoretically Determined Profiles of OH for a Water Vapor Mixing Ratio of  $7 \times 10^{-6}$  at 50 km.

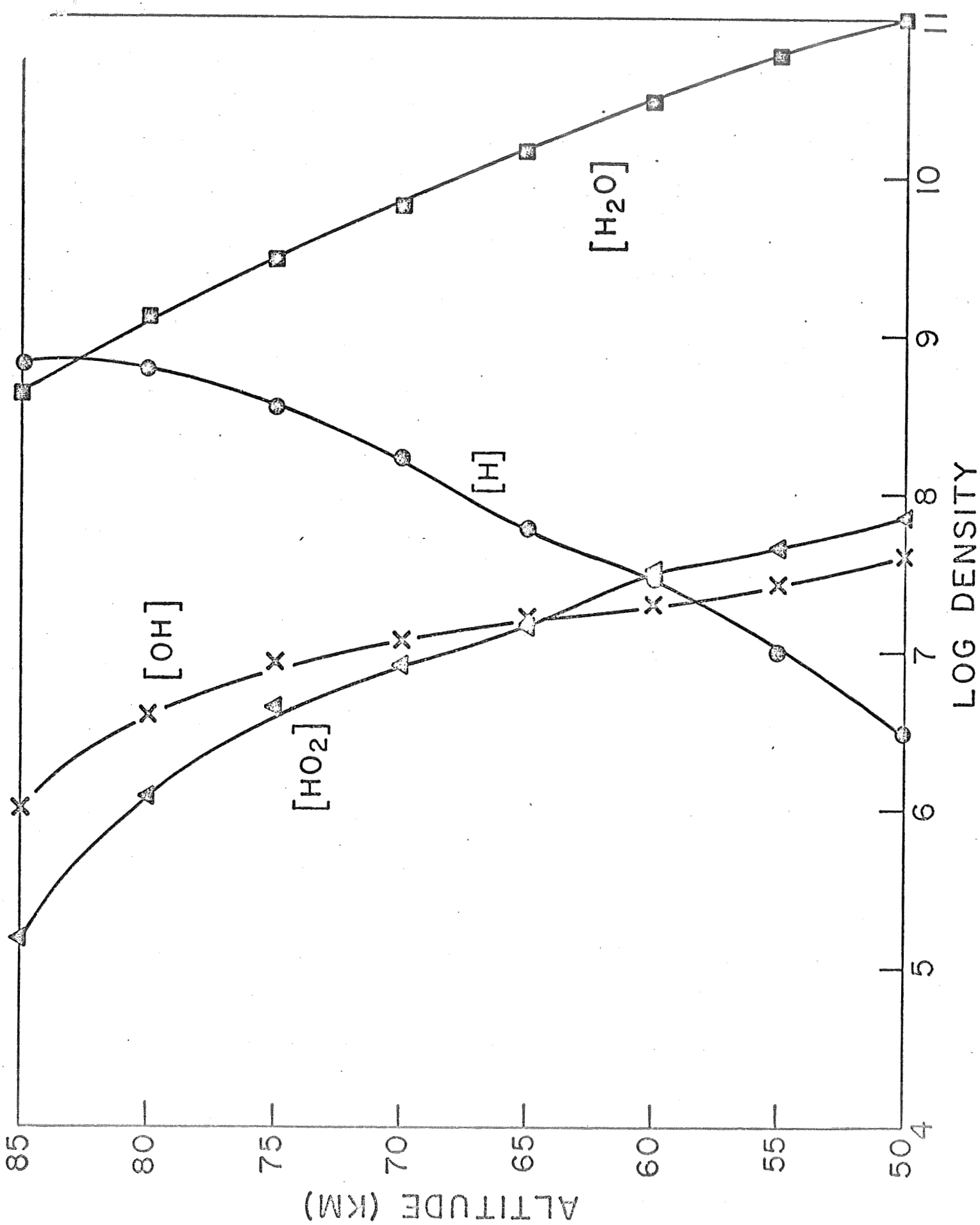


Fig. 19

Model of the reactive hydrogen constituents between 65 and 85 km for an eddy diffusion coefficient of  $1 \times 10^6 \text{ cm}^2/\text{sec}$